



HAL
open science

Constraining the Surface Flux of Sea Spray Particles From the Southern Ocean

Sean Hartery, D. Toohey, L. Revell, K. Sellegri, P. Kuma, M. Harvey, A. J
McDonald

► **To cite this version:**

Sean Hartery, D. Toohey, L. Revell, K. Sellegri, P. Kuma, et al.. Constraining the Surface Flux of Sea Spray Particles From the Southern Ocean. *Journal of Geophysical Research: Atmospheres*, 2020, 125 (4), 10.1029/2019JD032026 . hal-03207006

HAL Id: hal-03207006

<https://hal.science/hal-03207006>

Submitted on 23 Apr 2021

HAL is a multi-disciplinary open access archive for the deposit and dissemination of scientific research documents, whether they are published or not. The documents may come from teaching and research institutions in France or abroad, or from public or private research centers.

L'archive ouverte pluridisciplinaire **HAL**, est destinée au dépôt et à la diffusion de documents scientifiques de niveau recherche, publiés ou non, émanant des établissements d'enseignement et de recherche français ou étrangers, des laboratoires publics ou privés.

Constraining the Surface Flux of Sea Spray Particles from the Southern Ocean

S. Hartery¹, D. Toohey², L. Revell¹, K. Sellegri³, P. Kuma¹, M. Harvey⁴, A. J. McDonald¹

¹University of Canterbury, Christchurch, New Zealand

²University of Colorado Boulder, Boulder, Colorado, USA

³Laboratoire de Météorologie Physique (LaMP), CNRS/UCA, Aubière, France

⁴National Institute of Water & Atmospheric Research, Wellington, New Zealand

Key Points:

- Current-era GCMs over-estimate sea spray concentrations relative to measurements in the Ross Sea
- Better constraints for sea spray flux were found by tuning wind-speed based parameterizations to these observations
- Variations in sea surface temperature did not explain further variability within the temperature range studied

Corresponding author: Sean Hartery, hartery.s.p@gmail.com

Abstract

Modeling the shortwave radiation balance over the Southern Ocean region remains a challenge for Earth system models. To investigate whether this is related to the representation of aerosol-cloud interactions, we compared measurements of the total number concentration of sea spray generated particles within the Southern Ocean region to model predictions thereof. Measurements were conducted from a container laboratory aboard the R/V *Tangaroa* throughout an austral summer voyage to the Ross Sea. We used source-receptor modeling to calculate the sensitivity of our measurements to upwind surface fluxes. From this approach, we could constrain empirical parameterizations of sea spray surface flux based on surface wind speed and sea surface temperature. A newly tuned parameterization for the flux of sea spray particles based on the near-surface wind speed is presented. Comparisons to existing model parameterizations revealed that present model parameterizations led to over-estimations of sea spray concentrations. In contrast to previous studies, we found that including sea surface temperature as an explanatory variable did not substantially improve model-measurement agreement. To test whether or not the parameterization may be applicable globally, we conducted a similar regression analysis using a database of in situ whitecap measurements. We found that the key fitting parameter within this regression agreed well the parameterization of sea spray flux. Finally, we compared calculations from the best model of surface flux to boundary layer measurements collected onboard an aircraft throughout the Southern Ocean Clouds, Radiation, Aerosol Transport Experimental Study (SOCRATES), finding good agreement overall.

1 Introduction

In the remote boundary layer of the Southern Ocean, continental sources of particulate matter such as black carbon, terrestrial monoterpenes, dusts, and pollen contribute very little to the population of suspended particulate (Murphy et al., 1998). As a result, the magnitudes of the direct and indirect shortwave radiative effects from the suspended particulate within the region are largely driven by local, marine sources (Carslaw et al., 2013; McCoy et al., 2015). There has been a considerable amount of work in recent years to understand the excess of shortwave radiation reaching the ocean surface in the Southern Ocean within climate-chemistry models (CCMs), especially regarding the representation of clouds within these models (Trenberth & Fasullo, 2010; Bodas-Salcedo et al., 2014). Since hygroscopic particulate matter are a necessary precursor to cloud formation, they can indirectly exert a substantial influence on the radiation balance through modification of cloud brightness (Twomey, 1977) and cloud phase through the availability of ice nuclei (DeMott et al., 2010).

The natural sources of airborne particles in the region are the production of sea-spray generated particles (SSPs) from wind-wave interactions and ultra-fine particles from the homogeneous nucleation of sulfuric acid and other volatile vapours. However, the rate of production of SSPs remains an open problem: the number of particles entering the atmosphere of a given droplet size and at a given wind speed has been shown to vary by over an order of magnitude among existing parameterizations for the production of SSPs (Ovadnevaite et al., 2014). If one also accounts for the uncertainties related to predicting the dependence of the surface flux on the wind speed over the water, estimates for the intensity of the surface flux diverge further. As a result, both the concentration and seasonal cycle of SSPs remain poorly constrained in the Southern Ocean (Henzing et al., 2006; Revell et al., 2019). Several studies have shown that the lack of prediction accuracy for the flux of SSPs results in large biases between observed and modelled mass concentrations of SSPs in

67 the marine boundary layer (MBL), particularly in regions with cold waters (Jaeglé
68 et al., 2011; Grythe et al., 2014; Witek et al., 2016).

69 In general, sea spray is the dominant source of particulate matter in the South-
70 ern Ocean in terms of mass (Murphy et al., 1998); however, during ice formation in
71 coastal Antarctica, wind-blown frost flowers and snow from sea-ice can also become
72 locally prominent sources (Kaleschke et al., 2004; Yang et al., 2008). Since these
73 particles are the largest in the region (Quinn et al., 2017), they are also a substantial
74 contributor to the local aerosol optical depth (AOD) (Shindell et al., 2013). While
75 the contribution of SSPs to the regional AOD is much more significant than its con-
76 tribution to cloud albedo in the Northern Hemisphere, over the Southern Ocean it
77 is precisely the opposite (Ayash et al., 2008). This highlights that SSPs are a re-
78 gionally important component of cloud formation over the Southern Ocean. This is
79 not surprising: SSPs are mainly comprised of highly soluble sea salt and so they are
80 very efficient cloud condensation nuclei (CCN) (Petters & Kreidenweis, 2007). While
81 SSPs form only a small fraction of CCN globally, they can make up $\sim 65\%$ of CCN
82 over the Southern Ocean (Quinn et al., 2017).

83 Recent studies have also shown that SSPs can act as ice nucleating particles
84 (INPs), which encourage the phase transition of cloud droplets to ice (DeMott et
85 al., 2016; McCluskey et al., 2018). Since the Southern Ocean is far removed from
86 continental sources of INPs (e.g. dust), SSPs may be the only source of INPs in
87 the region. Ice nucleation sites within the droplets are likely a result of suspended
88 amounts of organic material within the sea surface microlayer which became en-
89 trained within the droplets during formation (DeMott et al., 2016). However,
90 organic materials form very little of the mass composition of the resulting SSPs
91 (Murphy et al., 1998); hence, the ice-nucleating potential of sea spray is very weak
92 relative to continental sources such as mineral dusts (McCluskey et al., 2018). Still,
93 the capacity for SSPs to modulate cloud phase represents an additional mechanism
94 through which they can affect the local radiation balance.

95 While we have emphasized the potential radiative effects SSPs might have
96 on the Southern Ocean region, there are other ways in which they can perturb the
97 Earth system. Several studies have shown that the largest SSPs are non-negligible
98 contributors to the exchange of latent and specific heat across the ocean–atmosphere
99 interface (Richter & Sullivan, 2013; Ortiz-Suslow et al., 2016). In a bulk flux model
100 of the air–sea exchange of heat, Andreas et al. (2015) showed that these large,
101 “shear” sea-spray droplets accounted for fluxes of sensible and latent heat on the
102 same order of magnitude as fluxes directly from the ocean–atmosphere interface
103 at high wind speeds ($U_{10} > 15 \text{ m s}^{-1}$). Observations and model simulations have
104 shown that the rate of momentum transferred from the atmosphere to the ocean
105 starts to decrease after a critical threshold wind speed is passed (30 m s^{-1} ; (Powell
106 et al., 2003; Bao et al., 2011; Hwang, 2018)). Theoretical work has suggested that
107 this change is driven by the exchange of sensible heat between the largest droplets
108 and the atmosphere, which become more abundant at high wind speeds (Bao et al.,
109 2011). This leads to considerable biases in the prediction of storm intensity (Bao et
110 al., 2011). The ability to predict the abundance of SSPs is therefore vital to fully
111 understanding many macroscopic processes within the region.

112 To constrain the potential role sea spray may have on the regional radiation
113 budget, it is first necessary to validate current parameterizations for its flux against
114 in situ observations of its abundance. However, there is currently a dearth of such
115 observations over the Southern Ocean. In this work we present measurements of
116 the total number concentration of airborne particles recorded throughout an austral
117 summer voyage to the Ross Sea aboard the R/V *Tangaroa*. We use these mea-
118 surements to test existing empirical parameterizations which describe the flux of
119 particles from wave breaking events in open seas. Measurements from instruments

120 onboard the High-Performance Instrumented Airborne Platform for Environmental
 121 Research (HIAPER) throughout the Southern Ocean Clouds, Radiation, Aerosol
 122 Transport Experimental Study (SOCRATES) were also used to validate these pa-
 123 rameterizations. Since the winds throughout both of these experiments included the
 124 extremes of surface conditions encountered at the air–sea interface, understanding
 125 the flux of SSPs in this highly dynamic region will be valuable in constraining both
 126 current and future flux estimates.

127 2 Methods

128 2.1 Measurements

129 The voyage aboard the R/V *Tangaroa* began on February 9th and ended on
 130 March 21st, 2018 departing and returning to Wellington, New Zealand (41°17' S,
 131 174°46' E). The bulk of the voyage was spent in waters south of 60°S, with 17 days
 132 of the voyage spent in seas between 60–70°S and 13 days of the voyage south of
 133 70°S.

134 In situ measurements of boundary layer aerosol were conducted from a con-
 135 tainer laboratory on the shelter deck of the R/V *Tangaroa* (2 m a.s.l.). The instru-
 136 ments within the container laboratory drew a continuous air sample through 40 m of
 137 100 mm ID anti-static tubing (EOLU PU; IPL Ltd.) from the mast of the R/V *Tan-*
 138 *garoa* (15 m a.s.l.). For the purposes of this study, we have primarily focussed on
 139 measurements from the passive cavity aerosol spectrometer probe (PCASP-100X;
 140 Droplet Measurement Technologies) with supplementary data from a differential
 141 mobility particle sizer (DMPS; TSI). The PCASP-100X is an optical particle counter
 142 which measured the number concentration size spectra of particles within the air
 143 sample. The instrument is capable of detecting particles with optical diameters
 144 between 0.1–3.0 μm in 30 size bins at 1 Hz. The DMPS measured the number con-
 145 centration size spectra of particles within the air sample with mobility diameters
 146 between 0.02–0.3 μm in 32 size bins once every 10 minutes. We have corrected
 147 the number concentration measurements according to calculations of the sampling
 148 and transport efficiency from Brockman (2001). These calculations accounted for
 149 anisokinetic sampling conditions, diffusion of the particles toward the tube walls,
 150 and gravitational settling of the particles. All of these calculations were based on
 151 empirical parameterizations of these losses in a turbulent flow. Across the spectrum
 152 of sizes we measured, we estimate that the total sampling efficiency was at most
 153 93%, but no less than 90%.

154 Throughout the voyage, a cavity ring-down spectrometer (CRDS; Picarro
 155 G2301) measured mole fractions of CO₂, CH₄, and H₂O from a separate sampling
 156 line. The sampling line of the CRDS was within 5 m of the main sampling line used
 157 for the particulate sampling. Intrusions of ship exhaust from the rear of the ship
 158 would have been sufficiently well-mixed in the turbulent air around the ship super-
 159 structure so as to affect both sampling lines. We used a threshold limit of 405 ppm
 160 of CO₂ to detect when ship exhaust contaminated our main sampling line. This
 161 threshold was well above the trend line of the [CO₂] mole fraction time-series. After
 162 removing these outliers, we used 1 Hz sub-samples of the particle number concen-
 163 trations to calculate 1-minute averages of the number concentration size spectra and
 164 its standard deviation. When the standard deviation of the 1 Hz samples deviated
 165 significantly from Poisson counting statistics the sample was removed.

166 This study also incorporated measurements from the New Zealand Met Ser-
 167 vice’s Automated Weather Station (AWS) aboard the R/V *Tangaroa*. The AWS
 168 anemometer was positioned at 22.5 m a.s.l. on the mast of the ship, while the rest
 169 of the AWS was positioned at 15 m a.s.l. The AWS measured: atmospheric pres-

170 sure, atmospheric temperature, relative humidity, wind speed, wind direction, and
 171 accumulated precipitation. Measurements of the average relative wind speed and
 172 wind direction were made using a pair of ultrasonic anemometers (Gill WindSonic)
 173 and reported at 1-minute intervals. The measurements of wind speed were corrected
 174 according to directionally-dependent acceleration factors, based on a model of air
 175 flow around the R/V *Tangaroa*'s superstructure (Popinet et al., 2004; Smith et al.,
 176 2011). The wind speeds were then corrected according to the ship heading and speed
 177 to derive the true wind speed and wind direction. Finally, the acceleration-corrected,
 178 true wind speed at 22.5 m was scaled to the 10 m reference level using the bulk flux
 179 algorithms developed from the Coupled Ocean-Atmosphere Response Experiment
 180 (COARE) (Edson et al., 2013). In employing the COARE bulk flux algorithms, we
 181 have not accounted for differences in the height of the AWS due to heave with re-
 182 spect to mean sea level, which may amount to ± 4 m in heavy seas. If for a given
 183 measurement, the pitch or roll of the ship was significant with respect to the mean
 184 wind vector, then the measured wind speed would have been systematically biased
 185 low. However, throughout the voyage, the pitch of the ship was $< 20^\circ$, and so these
 186 corrections would be less than 6%.

187 Measurements of the boundary layer number concentration size spectra were
 188 also conducted onboard HIAPER, a modified Gulfstream V aircraft, from January
 189 16th–February 24th, 2018. These measurements were part of the SOCRATES ex-
 190 periment. Over the course of the experiment, there were 15 flights, which departed
 191 and returned to Hobart, Australia. We have focused on the flights which coincided
 192 with our observational record, namely Research Flights (RF) 10–15 which took
 193 place between February 7th–24th, 2018. Two Ultra-High Sensitivity Aerosol Spec-
 194 trometers (UHSAS; Droplet Measurement Technologies) were used throughout the
 195 experiment to measure the number concentration size spectra of particles within the
 196 surrounding air; however, for this study we focused solely on the measurements from
 197 the UHSAS mounted inside of the aircraft. The UHSAS sampled ambient air via a
 198 counterflow virtual impactor inlet mounted outside of the aircraft. This ensured that
 199 the internal flow rate of the UHSAS was isokinetically matched to the exterior flow
 200 around HIAPER. Like the PCASP-100X, the UHSAS is an optical particle counter
 201 which can detect particles with optical diameters between 0.059–1.022 μm in 100
 202 discrete size bins at 1 Hz. It was determined that corrections to the number concen-
 203 tration size spectra from the additional ram pressure of sampling the aerosol from a
 204 moving aircraft would amount to less than 1%. This was substantially less than the
 205 observed variability in both the number concentration time series and the volume
 206 flow rate of the pump that provided the flow through the UHSAS. For each flight
 207 we identified 3–6 periods when the altitude was stable, there was little precipitation,
 208 and the observed number concentration size spectra were relatively stable. In each
 209 of these periods, we averaged the number concentration size spectra over 5–10 min-
 210 utes. This resulted in 28 unique measurements between 69–6,100 m a.s.l, 17 of which
 211 were in the boundary layer.

212 2.2 FLEXPART-WRF

213 The FLEXPARTicle transport model (FLEXPART), FLEXPART-WRF,
 214 is a Lagrangian particle dispersion model designed to model particle trajectories
 215 within mesoscale meteorological fields from the Weather Research & Forecasting
 216 Model (WRF) (Brioude et al., 2013). For this study, we used meteorological fore-
 217 casts from the real-time Antarctic Mesoscale Prediction System (AMPS) (Polar
 218 Meteorology Group, Byrd Polar and Climate Research Center, 2018). AMPS uses
 219 a variety of data sources to constrain these forecasts, including near-real-time sea-
 220 ice concentrations measured from the Special Sensor Microwave/Imager (SSM/I)
 221 radiometer and sea surface temperature (SST) data from the National Center for
 222 Environmental Prediction (NCEP) (Bromwich et al., 2005). Initial and boundary

223 conditions for AMPS were specified according to near-real-time forecasts from the
 224 NCEP Global Forecasting System (Bromwich et al., 2005). We used the AMPS
 225 output with the widest spatial coverage, domain 1, which has a horizontal resolu-
 226 tion of 24×24 km, a vertical resolution of 61 η levels, and a temporal resolution of
 227 three hours. The AMPS forecasts used throughout this study were downloaded from
 228 <https://www.earthsystemgrid.org/project/amps.html>.

229 We initialized 100, 000 particle trajectories from the geographic location of
 230 the R/V *Tangaroa* every three hours to match the temporal resolution of AMPS.
 231 Additional simulations were run for every hour in between the meteorological time
 232 steps if the R/V *Tangaroa* had entered a new grid cell in the AMPS domain. These
 233 two criteria resulted in 651 unique simulations. To trace losses due to deposition
 234 throughout the simulation, FLEXPART assigned each particle a unit mass dis-
 235 tributed over a log-normal size distribution. To match our observations, we centered
 236 this distribution around a geometric dry diameter of $0.20 \mu\text{m}$ ($D_{p,g} = 0.4 \mu\text{m}$ at
 237 80% relative humidity), with a geometric standard deviation of 2.00, and a dry den-
 238 sity of 1.84 g cm^{-3} . FLEXPART-WRF used the discretized Langevin equation to
 239 describe the turbulent dispersion of these particles through the atmosphere in re-
 240 verse time with an adaptive time-step strictly less than 180 s. The particles were
 241 advected through the meteorological fields specified by AMPS from the time of mea-
 242 surement up to five days prior in reverse time. Throughout the trajectory, losses
 243 of particle mass due to dry deposition were calculated according to the resistance
 244 method (Hicks et al., 1987). To improve these calculations we modified FLEXPART-
 245 WRF to account for hygroscopic particle growth according to the ambient relative
 246 humidity (Gerber, 1985), since changes in particle size can significantly affect a
 247 particle’s settling velocity and dry deposition velocity. FLEXPART-WRF also ac-
 248 counted for losses of particle mass from precipitation and droplet activation. Within
 249 clouds, FLEXPART-WRF calculated the scavenging rate of particles from droplet
 250 activation according to the parameterization of Hertel et al. (1995). For scavenging
 251 by precipitation below cloud, loss rates were estimated from the following empirical
 252 relationship:

$$253 \quad \Lambda = AI_s^B \quad (1)$$

254 where the scavenging rate, Λ , was calculated as a function of the rain-equivalent
 255 snow intensity, I_s (mm hr^{-1}), and user-set scavenging coefficients, A and B. While
 256 fairly good representations of particle scavenging from rain exist in the litera-
 257 ture, there is substantially more uncertainty with regards to the scavenging from
 258 snow (Slinn, 1977). Recent parameterizations of below-cloud scavenging in the non-
 259 WRF version of FLEXPART recommend applying an empirical fit to a set of snow
 260 scavenging rates measured in southern Finland (Kyrö et al., 2009; Grythe et al.,
 261 2017). However, this parameterization doesn’t explicitly account for increases in
 262 scavenging with increasing snow intensity. We observed that the differences in scav-
 263 enging rates Kyrö et al. (2009) observed across the particle size spectra were small
 264 compared to the difference in median snow scavenging rates they observed between
 265 their median observed snow intensity (0.2 mm hr^{-1}) and peak snow intensity (5
 266 mm hr^{-1}). We used the median scavenging rates and snow intensity values they
 267 reported to estimate the following scavenging coefficients for snow: $A = 4 \times 10^{-5}$
 268 and $B = 0.43$. For reference, the typical values used by FLEXPART-WRF for rain
 269 are 5×10^{-6} and 0.62, respectively. Together with the dry deposition velocity, the
 270 mass concentration loss rate could be described at any point in the simulation by
 271 the following:

$$272 \quad \frac{dm}{dt} = - \left(\frac{v_d}{h} + \Lambda \right) m \quad (2)$$

273 where m is the mass of the particle, v_d is the dry deposition velocity, and h was the
 274 height of the layer in which dry deposition occurred (30 m a.s.l.).

275 In reverse mode, FLEXPART-WRF calculated the residence time of the parti-
 276 cles within the lowest 100 m of the atmosphere. The residence time calculation was
 277 weighted by the local air density and the residual mass of the particles within the
 278 grid-cell. The weighted residence time was normalized by the initial mass of the par-
 279 ticles such that the resulting residence time accounted for losses from wet and dry
 280 deposition as described above. Finally, FLEXPART-WRF integrated the weighted
 281 residence time over the duration of the meteorological time-step for each grid-cell of
 282 the AMPS domain.

283 2.3 Quantifying the contribution of sea spray

284 Previous studies have shown that in pristine marine environments, the contri-
 285 bution of SSPs to the number concentration size spectra can be characterized by a
 286 single log-normal number concentration size distribution (Modini et al., 2015; Quinn
 287 et al., 2017). Distributions derived from this method have been shown to agree well
 288 with number concentration size spectra measured during laboratory wave-breaking
 289 experiments and the “canonical sea spray size distribution” derived from other
 290 studies (Prather et al., 2013; Lewis & Schwartz, 2004). This also agrees with the
 291 mass composition of the particles measured in the Southern Ocean boundary layer
 292 during the ACE-1 campaign, which found that particles larger than 0.3 μm were
 293 composed almost entirely of sea-salt (Murphy et al., 1998). We applied this method-
 294 ology to our own measurements of the number concentration size spectra from the
 295 PCASP-100X; i.e. we fit a number concentration size spectra, $dn(d \log D_p)^{-1}$, of the
 296 following form:

$$297 \frac{dn}{d \log D_p} = \frac{N}{\sqrt{2\pi} \log(\sigma_g)} \exp \left[-\frac{\log^2 \left(\frac{D_p}{D_{p,g}} \right)}{2 \log^2(\sigma_g)} \right] \quad (3)$$

298 where D_p is the particle diameter, N is the total number concentration of particles,
 299 $D_{p,g}$ is the geometric mean diameter of the distribution, and σ_g is the geometric
 300 standard deviation of the distribution. After fitting, the retrieved spectra were cor-
 301 rected to a relative humidity of 80% (Gerber, 1985). In the process of fitting, the
 302 geometric standard deviation (σ_g) of the mode was fixed to a value of 2, which best
 303 fit our data. While Modini et al. (2015) and Quinn et al. (2017) allowed σ_g to freely
 304 vary in their regression analysis, the variance-covariance matrix from our regression
 305 indicated that the resulting parameters were significantly correlated, since the data
 306 very weakly constrained σ_g .

307 To calculate the total number concentration of sea spray from the
 308 FLEXPART-WRF residence time, we assumed that the surface flux of SSPs also
 309 followed a log-normal distribution:

$$310 \frac{\partial f}{\partial \log D_p} = \frac{F}{\sqrt{2\pi} \log(\sigma_g)} \exp \left[-\frac{\log^2 \left(\frac{D_p}{D_{p,g}} \right)}{2 \log^2(\sigma_g)} \right] \quad (4)$$

311 where f is the partial particle flux in $\text{m}^{-2} \text{s}^{-1}$, F is the total particle flux in m^{-2}
 312 s^{-1} , and D_p is the particle diameter.

313 The most widely used empirical approach for constraining the particle flux
 314 from the ocean surface is the “whitecap method”. It results from the following as-
 315 sumptions: first, that the total flux of particles entering the atmosphere from the
 316 ocean surface can be determined from the fractional surface coverage of whitecaps,
 317 W (“whitecap fraction”); second, that the whitecap fraction can be adequately de-
 318 termined from the 10 m scalar wind speed over the ocean, U_{10} ; and third, that the
 319 shape of the SSP size distribution is not a function of wind speed. Laboratory and
 320 field experiments have shown that all of these assumptions are reasonable (Monahan

321 & Ó Muircheartaigh, 1980; Monahan et al., 1986). Hence, the total number of par-
 322 ticles entering the atmosphere, F , can be predicted from just the 10 m wind speed,
 323 U_{10} :

$$324 \quad \begin{aligned} F &= \frac{E}{\tau} W(U_{10}) \\ F &= \alpha W(U_{10}) \end{aligned} \quad (5)$$

325 where W is a function that models how the surface coverage of whitecaps increases
 326 as a function of wind speed, E is the number of particles produced per whitecap,
 327 and τ is the lifetime of the whitecaps. Since we can only hope to constrain one con-
 328 stant pre-factor, we combine both E and τ into a single parameter α , which we
 329 assume to be constant. Historically, the whitecap function W has been assumed
 330 to be a simple power-law, based on early field observations of whitecap forma-
 331 tion (Monahan, 1971). However, it has since been well-established that whitecaps
 332 do not form in the open ocean until the 10 m wind speed exceeds 3–4 m s⁻¹, which
 333 is a feature that cannot be described by a power-law model (A. Callaghan et al.,
 334 2008; Schwendeman & Thomson, 2015; Bell et al., 2017). We considered three other
 335 wind-dependent models of the surface flux that incorporated a threshold wind speed
 336 below which very few SSPs are produced:

$$337 \quad \begin{aligned} W_{PL} &= a_1 U_{10}^{a_2} \\ W_C(U_{10}) &= \begin{cases} b_1 (U_{10} - b_2)^3, & U_{10} \geq b_2 \\ 0, & U_{10} < b_2 \end{cases} \\ W_F(U_{10}) &= 1 - \Phi\left(\frac{c_1}{\sqrt{U_{10}}}\right) \\ W_{LLPL}(U_{10}) &= \frac{d_1 U_{10}^{d_2}}{1 + \left(\frac{U_{10}}{d_3}\right)^{-d_4}} \end{aligned} \quad (6)$$

338 where a_x, b_x, c_x and d_x and are empirical parameters determined from regression
 339 analysis with our observations, and Φ is the error function. The first function,
 340 W_{PL} (‘PL’ = ‘Power-Law’), is as previously introduced. The second function, W_C
 341 (‘C’ = ‘Cubic’), has been used to match more recent field observations of white-
 342 caps (A. Callaghan et al., 2008; Schwendeman & Thomson, 2015)). The third func-
 343 tion, W_F (‘F’ = ‘Fetch’), was based on the theoretical work of Snyder and Kennedy
 344 (1983), who developed a model of whitecap production based on a fetch dependent
 345 threshold for wave breaking. While the work of Xu et al. (2000) showed that the
 346 whitecap fraction could be fully determined from the model of Snyder and Kennedy
 347 (1983) if both the wind speed and fetch were known, the fetch was typically unlim-
 348 ited throughout our observation period. In high fetch regimes, the coverage of white-
 349 caps is only very weakly dependent on variations in fetch (Piazzola et al., 2002). As
 350 a result, we treated c_1 , which is a function of the fetch, as a free parameter to be
 351 determined through regression, since a single value should accurately describe the
 352 data. The last function, W_{LLPL} (‘LLPL’ = ‘Log-Logistic Power-Law’) combined
 353 the power-law with a log-logistic curve to emulate the threshold mechanism. While
 354 W_{PL} , W_C and W_{LLPL} predict that the surface flux will continue increasing as a
 355 function of wind speed, the Fetch model (W_F) is the only model which predicts that
 356 there exists an upper bound on the particle flux at high wind speeds.
 357

358 There has also been some debate as to how the temperature of the sea water
 359 might moderate whitecap formation (Mårtensson et al., 2003; Sellegri et al., 2006;
 360 Jaeglé et al., 2011; Zábori et al., 2012; A. H. Callaghan et al., 2014; Grythe et al.,
 361 2014). This was tested directly with SST data from NCEP, which was available
 362 from the AMPS forecasts. Thus, the model of surface flux was expanded to:

$$363 \quad \begin{aligned} F &= \alpha(T_w) W(U_{10}) \\ \alpha(T_w) &= \alpha_0 (1 + \alpha_1 T_w) \end{aligned} \quad (7)$$

364

365 where the coefficient α , which describes both the lifetime of the whitecaps and
 366 the number of particles produced per whitecap, is now a function of the SST, T_w .
 367 Note that, in reality, parameters α_0 and other scaling coefficients within W (e.g.
 368 a_1, b_1, d_1) cannot be determined independently, so they are combined into a single
 369 parameter for each regression (e.g. $a_1^* = a_1\alpha$). Finally, we assumed that the surface
 370 flux was well-mixed within the lowest atmospheric grid cell in FLEXPART-WRF, h
 371 = 100 m. Following these assumptions, the number concentration of particles in the
 372 SSP mode, \hat{N} , was calculated according to:

$$373 \quad \hat{N}_i = \frac{1}{h} \int_{-t_0}^0 \iint_O F(1 - C_{ice}) d\mathcal{P}_i \quad (8)$$

374 where t_0 was the length of the FLEXPART-WRF simulation, C_{ice} was the fractional
 375 surface coverage of sea ice, O denotes that the integral was only integrated over
 376 oceans, and \mathcal{P}_i was the map of footprint residence times for the observation i .

377 A non-linear least-squares regression analysis optimized the set of parameters
 378 for each surface flux model, W , being tested. Parameter optimization was achieved
 379 with the Gauss-Newton algorithm, where the goodness-of-fit was measured by the
 380 Nash-Sutcliffe model efficiency coefficient (NSE):

$$381 \quad NSE = 1 - \frac{\sum_{i=1}^m (N_i - \hat{N}_i)^2}{\sum_{i=1}^m (N_i - \bar{N})^2} \quad (9)$$

382 where m was the total number of observations and \bar{N} represents the average of ev-
 383 ery measurement of N_i within the dataset (Nash & Sutcliffe, 1970). To account for
 384 differences between the number of parameters between models, we also calculated
 385 the Akaike Information Criterion (AIC), which penalized models with more param-
 386 eters (Akaike, 1974):

$$387 \quad AIC = 2k + m \log \left(\frac{1}{m} \sum_{i=1}^m (N_i - \hat{N}_i)^2 \right) \quad (10)$$

388 where k was the total number of parameters for a given model. The best model of
 389 surface flux was the model which minimized the AIC.

390 **3 Results**

391 **3.1 Comparisons Between Surface Meteorological Measurements** 392 **and Model Forecasts**

393 To demonstrate that the transport simulations produced a meaningful link
 394 between the observations and surface fluxes, it was necessary to first validate the
 395 Antarctic Mesoscale Prediction System’s meteorological fields against the record of
 396 observations from the Automated Weather Station (AWS) aboard the R/V *Tan-*
 397 *garoa*. As described in the Section 2.1, the AWS measured wind speeds at 22.5 m,
 398 which were corrected to the 10 m reference height according to the COARE 3.5 bulk
 399 flux algorithms. The corrected wind speeds were compared to the 10 m wind speeds
 400 predicted by the AMPS forecasts by matching the location of the R/V *Tangaroa* to
 401 the nearest grid-cell within AMPS. This comparison is presented in Fig. 1. The cor-
 402 relation coefficients calculated for both the wind speed ($R = 0.81$) and wind direc-
 403 tion ($R_o = 0.78$) between observations and forecasts were both significant ($p < 0.01$),
 404 where R_o represents the circular correlation coefficient (Fisher & Lee, 1986).

405 Despite the good agreement we found between the measured and forecast
 406 winds, there was no spatio-temporal correlation between the rain-equivalent snow

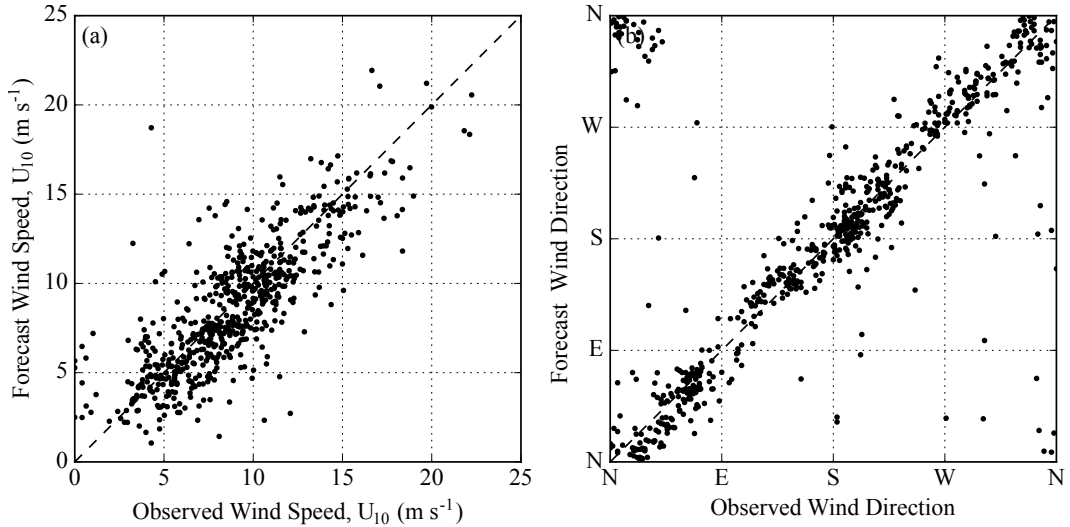


Figure 1. (a) The hourly 10 m scalar wind speeds from the AMPS forecasts were compared to the corrected wind speed (see Section 2.1) observed on the R/V *Tangaroa*. (b) The hourly 10 m wind direction.

407 rate measured aboard the R/V *Tangaroa* and the precipitation fields forecast by
 408 AMPS. However, the climatological distribution of the rain-equivalent snow rate was
 409 at least consistent between measurements and forecasts. This suggests that even if
 410 precipitation was not spatially consistent with our observations, it was at least as
 411 frequent, and of the right intensity within the AMPS forecasts. While comparing
 412 localized, discrete events like precipitation can be challenging, even comparing our
 413 measurements to grid cells within 100 km and within 6 hours of the R/V *Tangaroa*
 414 measurements did not produce a significant correlation.

415 3.2 Source–Receptor Modeling

416 In Fig. 2a we show the cumulative five-day, near-surface, residence time for
 417 all of the source–receptor simulations described in Section 2.2. The track of the
 418 R/V *Tangaroa* throughout the voyage has also been shown for reference. As ex-
 419 pected, the near-surface residence time was greatest near the R/V *Tangaroa*. This
 420 indicated that our measurements were most sensitive to surface fluxes near the ship.
 421 To understand how dry deposition might govern the concentration of SSPs, we also
 422 ran several FLEXPART-WRF simulations in which the dry deposition velocity was
 423 set to a fixed rate. However, the consistent turbulence of the atmosphere over the
 424 Southern Ocean meant that the simulated particles were often very evenly dispersed
 425 throughout the boundary layer. As a result, dry deposition was severely limited
 426 throughout all of the simulations. Predicted surface flux sensitivities within these
 427 simulations only began to diverge after 1–2 days had elapsed in simulation time;
 428 however, by then the residence time was typically less than 5% of what it was near
 429 the ship. Hence, dry deposition was not a strong factor controlling the concentration
 430 of SSPs.

431 It was evident from Fig. 2a, however, that our observations near the Ross Ice
 432 shelf were sensitive to non-marine sources. The fraction of the time the particles
 433 spent above non-marine surfaces throughout their five-day simulations increased
 434 rapidly as the R/V *Tangaroa* approached Cape Adare, Antarctica. Throughout this
 435 period we observed strong, southerly winds, which brought continental, Antarctic air

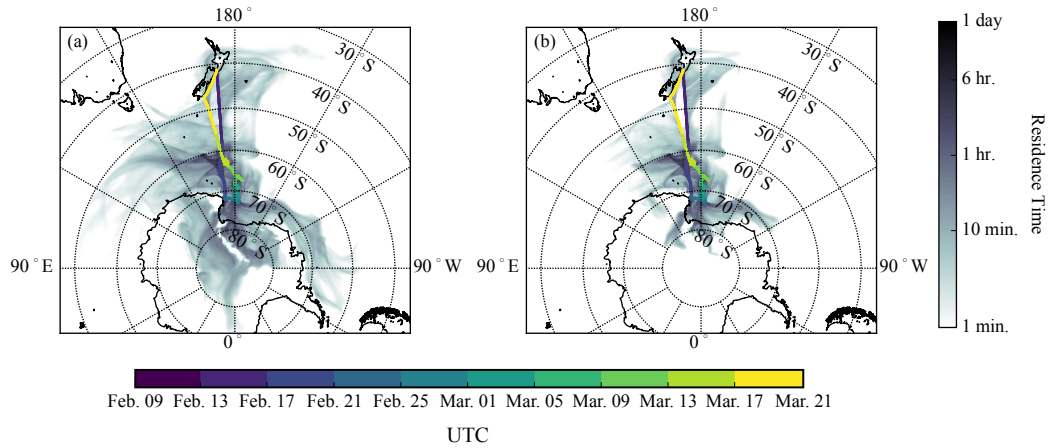


Figure 2. (a) A map of the cumulative near-surface residence time derived from FLEXPART-WRF particle dispersion simulations. The model simulated the transport of 1×10^5 $0.2 \mu\text{m}$ particles in reverse time from the time of measurement to five days prior. The near-surface residence time is simply the total amount of time the particle spent below 100 m a.g.l. Within FLEXPART-WRF the transport of the particles was calculated according to meteorological forecasts from the Antarctic Mesoscale Prediction System (AMPS). (b) The same map, but now for a 48-hr. simulation. The colored line in both panels marks the track of the R/V *Tangaroa* throughout the voyage.

436 across the Ross Ice Shelf. Intrusions of continental air into the MBL are a common
 437 phenomenon within the region (Coggins et al., 2014; Coggins & McDonald, 2015).
 438 Near the end of the observation period, after March 18th, 2018, the source-receptor
 439 simulations showed that our measurements were also sensitive to surface fluxes from
 440 the South Island of New Zealand. This was a direct result of the strong northerlies
 441 we observed throughout our return transect.

442 As we identified in Section 3.1, the rain-equivalent snow rates forecast by
 443 AMPS were not well-correlated with snowfall intensity measured onboard the R/V
 444 *Tangaroa*. While the frequency of occurrence of these events seemed consistent, it
 445 is important to note that the wet deposition scheme used by FLEXPART-WRF
 446 implicitly assumed that in-cloud activation events only occurred within a precipitat-
 447 ing cloud. Hence, the frequency of in-cloud scavenging events was almost certainly
 448 under-estimated within the source-receptor simulations. As Hertel et al. (1995)
 449 note, the magnitude of the loss of particles to in-cloud activation is almost always
 450 greater than either below-cloud scavenging or dry deposition. In fact, an activation
 451 event is always strong enough to terminate a particle trajectory within FLEXPART-
 452 WRF. Therefore, it was expected that the source-receptor modeling vastly over-
 453 estimated the near surface residence time by continuing to advect particles that
 454 should have been completely scavenged by cloud. However, a lack of boundary
 455 layer cloud within the simulation did not stem from this issue alone. It has been
 456 well-established that there is currently a large shortwave radiation bias over the
 457 Southern Ocean (Bodas-Salcedo et al., 2014). Observations of cloud base height
 458 from radiosondes and ceilometer measurements throughout this same voyage showed
 459 that the shortwave radiation bias is related to the lack of low-level cloud and fog
 460 predicted within atmospheric models (Kuma et al., 2019). Therefore, it is reason-
 461 able to expect that even with an improved in-cloud activation scheme (e.g. Grythe
 462 et al. (2017)), FLEXPART-WRF still would have under-estimated the frequency
 463 of droplet activation events. This would have a substantial impact on our source-

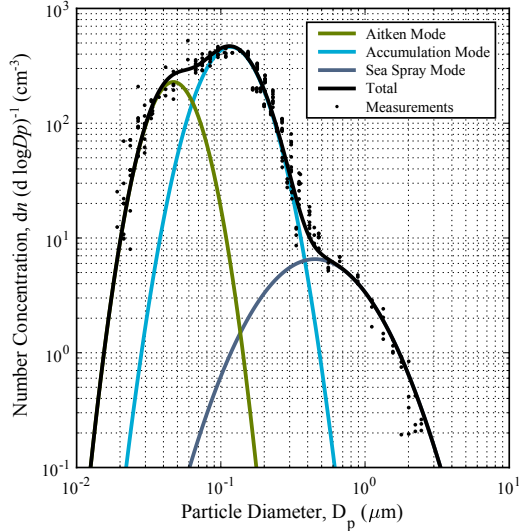


Figure 3. Number concentration size spectra measured from the PCASP-100X (0.1–3 μm) and the DMPS (0.02–0.3 μm) on February 20th, 2018 at 1300 UTC. Particle sizes have been corrected to 80% relative humidity (Gerber, 1985). Number concentrations for particles larger than 0.5 μm were used to constrain a single log-normal number concentration size distribution (“SSP mode”). This method has been used by other researchers (e.g. Modini et al. (2015) and Quinn et al. (2017)) to constrain the contribution of SSPs to the total number concentration size spectra. The Aitken and accumulation modes are shown for reference.

464 receptor calculations, resulting in significantly less ocean surface area contributing
 465 to the integral in Eq. (8). To visualize this effect, we have also shown the cumula-
 466 tive near surface residence time for a two-day simulation in Fig. 2b, instead of the
 467 five-day simulation shown in Fig. 2a. This is addressed further in Section 3.4.

468 3.3 Number Concentrations of Sea Spray

469 In Fig. 3 we show an example modal analysis of a number concentration size
 470 spectrum measured by the PCASP-100X and DMPS aboard the R/V *Tangaroa*. The
 471 size spectra were used to constrain three log-normal “modes” which represented the
 472 entire size distribution. The largest of these modes, the SSP mode, is so-named as it
 473 has been shown to be comprised almost solely of SSPs (Modini et al., 2015; Quinn
 474 et al., 2017). At each hour of observation throughout the voyage we constrained the
 475 SSP mode from the spectral measurements shown in Fig. 3, resulting in the time
 476 series of the total number concentration of SSPs shown in Fig. 4. In general it was
 477 sufficient to constrain the SSP mode from just the PCASP-100X measurements,
 478 so the measurements from the DMPS were not used in this study, but are shown
 479 for reference. Throughout the entire voyage, we observed the median and standard
 480 deviation of the geometric mean diameter of the SSP mode to be $0.4 \pm 0.05 \mu\text{m}$
 481 at a relative humidity of 80%. This agreed well with the observations of Quinn et
 482 al. (2017) in the Southern Ocean. This also agreed with the median dry diame-
 483 ter of SSPs measured from laboratory generated waves, 140–200 nm (Prather et
 484 al., 2013), since SSPs are twice as large at 80% relative humidity compared to dry
 485 conditions (Gerber, 1985).

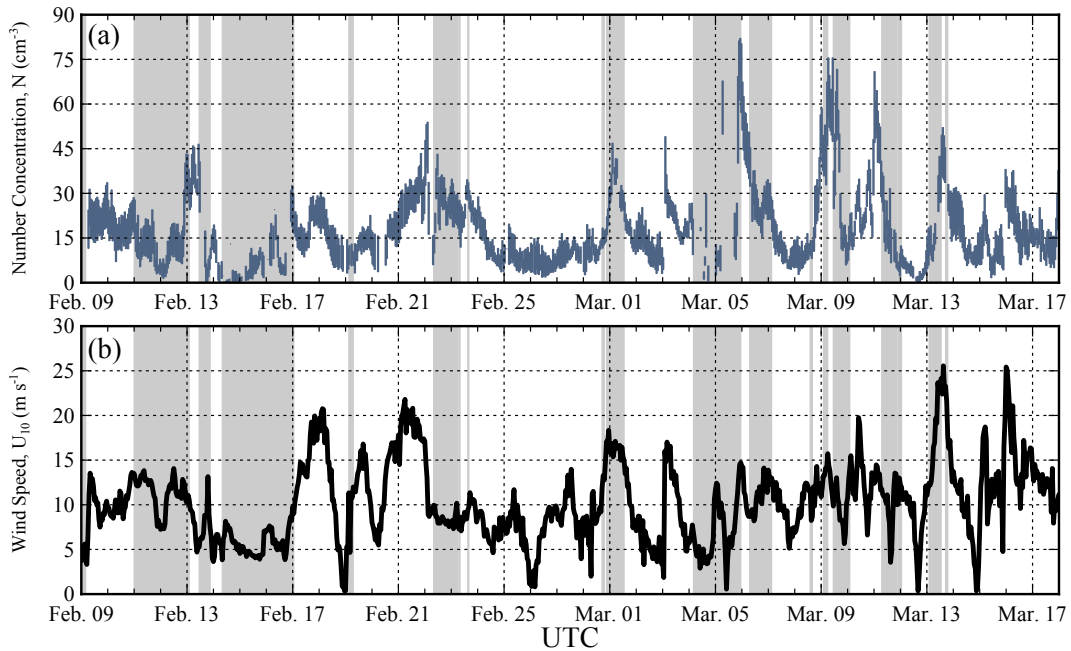


Figure 4. (a) The average hourly number concentration of sea spray particles is shown for the entire campaign with periods of fog ($RH > 98\%$) or rain ($> 1 \text{ mm hr}^{-1}$) marked by the shaded areas. (b) The hourly 10 m wind speed.

486 In Fig. 4a, the total number concentrations of SSPs and the 10 m scalar wind
 487 speeds measured are shown from the beginning of the voyage, February 9th, 2018,
 488 until March 18th, 2018. Throughout the voyage, there were several periods when
 489 either fog or precipitation was observed at the ship. As expected, fog very efficiently
 490 scavenged the particles in the SSP mode through droplet activation processes, much
 491 more so than precipitation. However, the lack of observed particles during such
 492 events meant that the SSP mode could not be constrained. This is particularly evi-
 493 dent around March 5th, 2018. In the last three days of the voyage, March 18th–21st,
 494 2018, we encountered strong northerly winds along the coast of New Zealand, which
 495 transported terrestrial particles to the R/V *Tangaroa*. The addition of these non-
 496 SSPs resulted in number concentration size spectra from which the SSP mode could
 497 not be constrained. As a result, measurements when fog or precipitation was ob-
 498 served at the ship, or when there was a significant influence from New Zealand were
 499 excluded from the regression analysis presented in the following section.

500 In Fig. 4b we also show the 10 m wind speed throughout the same period of
 501 measurement. We observed that when winds were light ($U_{10} < 4 \text{ m s}^{-1}$) the total
 502 number concentration of particles in the SSP mode was no more than 10 cm^{-3} , and
 503 had a median of 7 cm^{-3} . Light-wind periods ($U_{10} < 4 \text{ m s}^{-1}$) occurred 14% of the
 504 time in upwind conditions, as weighted by the near surface residence time. However,
 505 during a light-wind period on March 12th, 2018, there appeared to be no particles at
 506 all. This agreed well with the transport modeling in Fig. 2, which showed that dur-
 507 ing all light-wind periods, except the period occurring on March 12th, the particles
 508 had a significant near surface residence time over Antarctica. While the boundary
 509 layer over Antarctica is generally a very pristine environment, human activity from
 510 research stations near the Ross Ice shelf and exposed mountain faces both represent
 511 potential sources for the concentration of particles observed at low wind speeds. In
 512 the regression analysis that followed, the median concentration of SSPs observed at

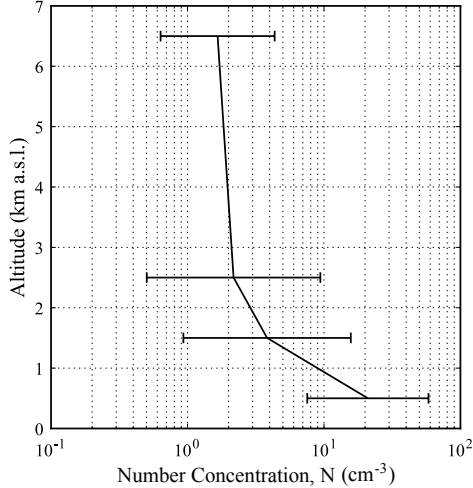


Figure 5. The total number concentration of sea spray generated particles is shown as a function of altitude over the course of several flights aboard HIAPER, (RF 11–15). The ranges within each altitude bin show the minimum and maximum number concentration observed. Flights RF 11–15 took place on the following days, in order: Feb. 17th, 18th, 20th, 21st and 24th, 2018.

513 low wind speeds was removed from the observations (except for the period around
 514 March 12th, 2018). After removing this background concentration, we calculated the
 515 hourly-averaged number concentration of particles in the SSP mode to be 9 cm^{-3} ,
 516 with a maximum of 62 cm^{-3} .

517 In Fig. 5 we show the total number concentration of SSPs derived from the
 518 UHSAS number concentration size spectra onboard HIAPER. These measurements
 519 were taken over the course of several flights in February 2018 to illustrate the range
 520 of concentrations observed within each 1 km bin. The measurements within one
 521 kilometer of the Earth’s surface were always determined to be below-cloud (if any
 522 cloud was present) and within the boundary layer. In contrast, all other bins were
 523 determined to be above cloud (if any cloud was present) and above the boundary
 524 layer. From Fig. 5 we can also identify that there was always at least $5\text{--}10 \text{ cm}^{-3}$ of
 525 SSPs in the boundary layer, which is consistent with the measurements at low wind
 526 speeds on board the R/V *Tangaroa*. As expected, there were also very few SSPs
 527 above the cloud, indicating that nearly all of these particles had been consumed
 528 during cloud formation.

529 3.4 Regression Analysis

530 Predicted SSP concentrations can be obtained by integrating Eq. (8); however,
 531 we have already identified that particle losses from in-cloud scavenging represented
 532 the greatest uncertainty to our source–receptor modeling. To address this within
 533 the regression analysis we allowed the simulation length, t_0 , to vary as a free pa-
 534 rameter within Eq. (8). In effect, this allowed the regression to estimate the return
 535 rate of a droplet activation event within a boundary layer cloud (e.g. fog or ma-
 536 rine stratocumulus) or a significant precipitation event ($>10 \text{ mm hr}^{-1}$). Either of
 537 these events would have efficiently scavenged the particle, thereby terminating its
 538 trajectory. This approach is similar to the Statistical Wet Deposition method used
 539 by other researchers, which prescribes the length of time it takes a surface flux of

540 particles to fully mix into the boundary layer after a precipitation event or cyclone
 541 (e.g. Ovadnevaite et al. (2014)).

Table 1. The values listed in this table are the relative likelihood that a given parameterization of surface flux correctly predicted the observed number concentration of sea spray generated particles relative to the best parameterization. These values were calculated from the difference between the Aikake Information Criterion (AIC) of each parameterization and the AIC of the best parameterization (AIC_b) according to the following: $\exp(-0.5(AIC - AIC_b))$ (Burnham & Anderson, 2002). The AIC measures the log-likelihood that a given surface flux parameterization minimizes the residual sum of squares between predicted and observed concentrations while also penalizing parameterizations which include large numbers of parameters (Akaike, 1974). See Eq (6) for parameterization definitions.

Surface Flux parameterization	W_{PL}^\ddagger	W_C^\dagger	W_F^\S	$W_{LLPL}^{\dagger\dagger}$
$F(U_{10})$	$<1 \times 10^{-3}$	$<1 \times 10^{-3}$	1	0.2
$F(U_{10}, T_w)$	$<1 \times 10^{-3}$	$<1 \times 10^{-3}$	0.6	$<1 \times 10^{-3}$

‡ Power-Law; † Cubic; § Fetch; †† Log-Logistic Power-Law.

542 In Table 1 we have calculated the relative likelihood that a given surface flux
 543 parameterization fit the data as compared to the best parameterization, W_F . We
 544 used the relative probabilities in Table 1 to compare two parameterizations: for in-
 545 stance, modelling the flux with W_F and a function of sea surface temperature was
 546 only 60% as likely to optimally fit our data as using W_F alone. We also found that
 547 regardless of the surface flux parameterization, the optimal simulation length, t_0 was
 548 48 ± 3 hours. This is similar to the “filling time” Ovadnevaite et al. (2014) used to
 549 characterize surface fluxes of SSPs from their measurements in the North Atlantic.
 550 The filling time is a characteristic timescale used in the Statistical Wet Deposition
 551 Method for determining sea spray fluxes from a concentration time series (Lewis &
 552 Schwartz, 2004). Definition of the filling time varies by author. In Ovadnevaite et al.
 553 (2014), they interpret the filling time as “...the time between the cyclone formation
 554 and subsequent arrival to [the measurement location]” instead of “the time since the
 555 last precipitation event as considered in (Lewis & Schwartz, 2004)”. The filling time
 556 we determined is consistent with the average time that elapsed between the passage
 557 of seven separate cyclones we encountered throughout March, 2018. These cyclones
 558 provided widespread high winds and boundary layer cloud, resulting in high fluxes,
 559 but relatively short lifetimes for any suspended particulate. Hence, our finding is
 560 consistent with the definition of filling time given by Ovadnevaite et al. (2014).

561 According to the AIC, the best parameterization for the surface flux of SSPs,
 562 F , used the fetch parameterization for whitecaps, W_F (Snyder & Kennedy, 1983; Xu
 563 et al., 2000):

$$\begin{aligned}
 \frac{\partial f}{\partial \log D_p} &= \frac{F}{\sqrt{2\pi} \log(2)} \exp \left[-\frac{\log^2 \left(\frac{D_p}{0.4} \right)}{2 \log^2(2)} \right] \\
 F &= \alpha W_F(U_{10}) \\
 \alpha &= 3.6 \times 10^7 \\
 W_F(U_{10}) &= 1 - \Phi \left(\frac{6.5}{\sqrt{U_{10}}} \right)
 \end{aligned}
 \tag{11}$$

566 where D_p is the particle diameter in μm at a relative humidity of 80%.

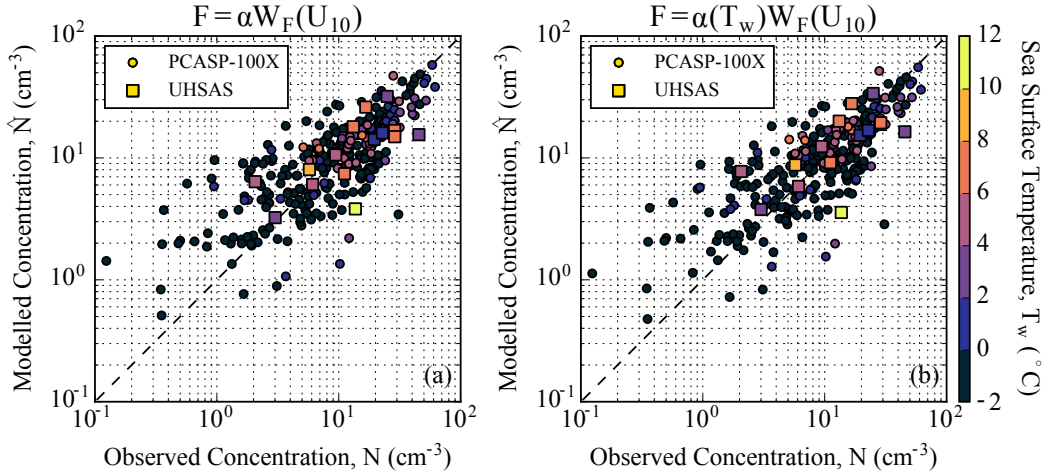


Figure 6. (a) Predicted concentrations of sea spray generated particles from the best parameterization of surface flux are compared to measurements from two observation platforms: a PCASP-100X aboard the R/V *Tangaroa* and the UHSAS onboard HIAPER. The best parameterization for the surface flux, F , of these particles was a function of the wind speed over the ocean surface. Each model–measurement pair is colored according to the average SST, weighted by the near-surface residence time. (b) As in (a), but for a parameterization of surface flux which incorporated a linear function of SST in addition to the wind speed dependence.

567 In Fig. 6a we show the model–measurement residuals for the best parameter-
 568 ization of surface flux. The model–measurement residuals have been color-coded
 569 according to the average SST. The average values of SST were weighted by the two-
 570 day, near-surface residence time. On average, the predicted concentrations did not
 571 appear to be biased positive or negative. However, a recent study by Jaeglé et al.
 572 (2011) showed that particle fluxes may significantly depend on SST. Changes in SST
 573 result in changes to the water viscosity. This is thought to modify the length of time
 574 for the whitecap to dissipate, τ , which is part of the constant, α . Hence, in order to
 575 compare to their result, we fit a linear correction term for the constant α presented
 576 in Eq. (11) as a function of the SST, T_w , finding:

$$577 \alpha(T_w) = 3.6 \times 10^7 (1 + 0.024T_w) \quad (12)$$

579 The model–measurement residuals of the temperature-corrected parameterization,
 580 are shown in Fig. 6b. From Table 1 we can see that this did not substantially
 581 improve model fidelity. In both Figs. 6a and b we have also shown the model–
 582 measurement pairs for the SOCRATES observations within the boundary layer.
 583 Since these measurements were not included within the regression framework, the
 584 good agreement in both of these figures provides a measure of confidence that
 585 Eq. (11) produces reasonable results within the Southern Ocean region.

586 In Fig. 7a we show the predicted flux of SSPs from each of the models in
 587 Eq. (6) as a function of near-surface wind speed. The total particle flux predicted
 588 by Gong (2003) has also been shown for reference. In Fig. 7b we have compared the
 589 linear function of SST we recovered from the regression analysis to the polynomial
 590 function fit by Jaeglé et al. (2011). We have shifted the values of the polynomial
 591 function so that it matches our linear function at $T_w = -2^\circ\text{C}$. The slope of our linear
 592 function predicts that SST is not as significant a control of SSP surface flux as
 593 shown by Jaeglé et al. (2011). This may be a result of the distribution of our mea-

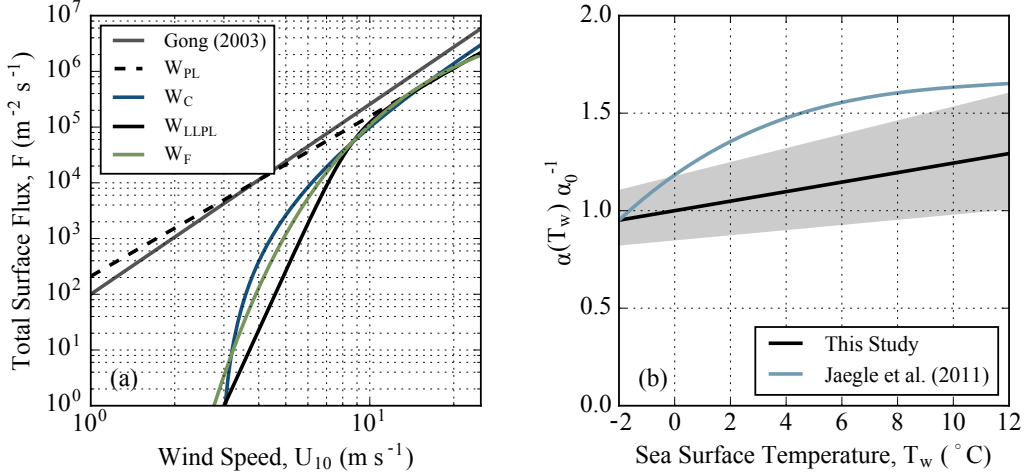


Figure 7. (a) The best parameterization of the total surface flux of sea spray generated particles, W_F , is compared to calculations from the Gong (2003) parameterization. (b) The linear bias correction function found by the regression is compared to the function reported by Jaeglé et al. (2011), where their function has been shifted vertically to match the linear bias correction function at $T = -2^{\circ} \text{C}$. The shaded region shows how uncertainty in the retrieved regression parameters propagated to prediction uncertainty.

594 measurements across different SST regimes since 78% of our observations were related
 595 to waters in a narrow temperature range (-2 – 0°C). Hence, there would be little im-
 596 provement to either the NSE or AIC for these samples. Still, as shown in Fig. 7b,
 597 the bias correction curve presented by Jaeglé et al. (2011) is clearly outside of the
 598 uncertainty bounds for the modest temperature dependence we observe within our
 599 dataset.

600 Finally, we compared the Nash-Sutcliffe model efficiency coefficient (NSE) for
 601 the best parameterization we found within our regression framework to two differ-
 602 ent parameterizations of SSP surface flux. The NSE is generally equivalent to R^2 ,
 603 but can also become negative when the average observed concentration provides a
 604 better fit to the data than the proposed parameterization. From Table 2 it is clear
 605 that Eq. (11) predicted concentrations of SSPs that were more consistent with our
 606 observations than predictions from either the Gong (2003) or the Jaeglé et al. (2011)
 607 parameterizations. Comparisons showed that the Gong (2003) parameterization
 608 produced too many SSPs at all wind speeds.

609 For reference, we also performed the regression for the entire five-day simula-
 610 tion. In all of the parameterizations presented, the NSE decreased significantly for
 611 the longer simulation, consistent with our hypothesis that in-cloud droplet activation
 612 was not accurately simulated. In addition, surface fluxes predicted by W_F when
 613 constrained by the five-day simulations were strictly smaller than surface fluxes pre-
 614 dicted by W_F when constrained by the two-day simulations, for all wind speeds.
 615 Therefore, our finding that the parameterization of Gong (2003) over-predicted the
 616 surface flux of SSPs was robust.

617 3.5 Meta-Analysis of Whitecap Data

618 In order to assess the conditions under which the parameterization presented
 619 above may be applicable, we analyzed global whitecap data from the literature. In

Table 2. The Nash-Sutcliffe model efficiency coefficient between the number concentration of SSPs predicted by a given surface flux parameterization and the observation conducted aboard the R/V *Tangaroa*. The time, t_0 , is the length of time for which the Lagrangian particle dispersion parameterization simulated the movement of SSPs back in time. A negative value for the NSE implied that the mean of the observations was better at predicting the observed variance than the given parameterization, whereas a value of 1 would imply a perfect model-measurement fit.

Surface Flux parameterization	NSE ($t_0 = 48$ hours)	NSE ($t_0 = 120$ hours)
(Gong, 2003)	<0	<0
(Jaeglé et al., 2011)	0.22	<0
Eq. (11)	0.67	0.52

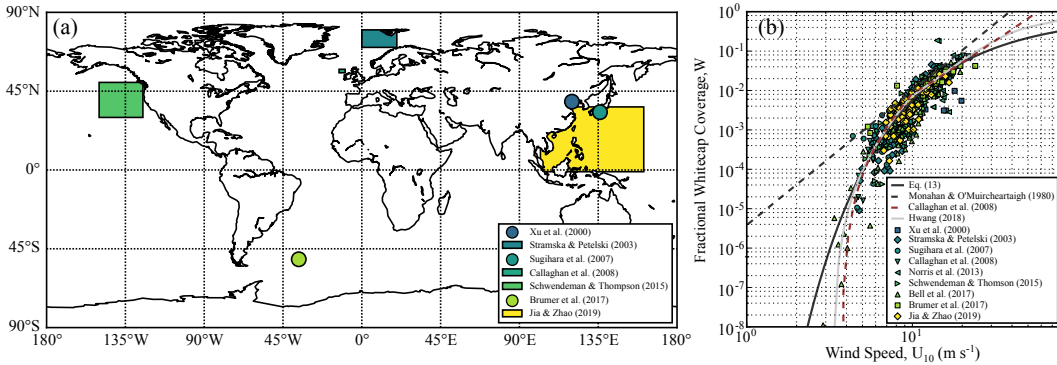


Figure 8. (a) The spatial extent of shipborne and tower whitecap observations within the database assembled for the whitecap meta-analysis. Studies where the coordinates of the observations were not specified all took place in the North Atlantic. (b) The fractional coverage of the sea surface by whitecaps as a function of 10 m wind speed.

Fig. 8b we have amalgamated 527 in situ ship-borne and tower observations of the surface coverage of whitecaps as a function of the 10 m wind speed, U_{10} (Xu et al., 2000; Stramska & Petelski, 2003; Sugihara et al., 2007; A. Callaghan et al., 2008; Norris et al., 2013; Schwendeman & Thomson, 2015; Bell et al., 2017; Brumer et al., 2017; Jia & Zhao, 2019). Studies published after the year 2000 were used since they all employed some form of automated image processing. This meant that each whitecap measurement was a result of $>10^2$ images, a necessary minimum to have a convergent mean (A. H. Callaghan & White, 2009). The spatial coverage of these studies is shown in Fig. 8a, indicating that there is a good degree of coverage across surface temperature regimes within the database. In Fig. 8b we have shown three parameterizations for the whitecap coverage from the literature overlying the in situ measurements (Monahan & Ó Muircheartaigh, 1980; A. Callaghan et al., 2008; Hwang, 2018). We used the AIC to compare the existing parameterizations shown in Fig. 8b to the fetch model, which was fit to the data via non-linear least-squares regression. We found that the fetch model for whitecap development captured the variability in the database best, with the relative likelihood that the other models accurately captured the variability being $<10^{-3}$. It also did so with a continuous function, whereas the other models were piece-wise. The best fit for the whitecap data was as follows:

$$W_F = 1 - \Phi \left(\frac{6.2}{\sqrt{U_{10}}} \right) \quad (13)$$

640 We also sought to validate the dependence of SSP fluxes on SST. However, SST data
 641 within the works cited were either not included or simply summarized as a range
 642 of values encountered. Still, most voyages made their measurements within a fairly
 643 narrow SST band. Hence, we could test whether or not there was any dependence
 644 by using a voyage-average SST for each study. Using the AIC as a measure of the
 645 goodness of fit, we found that SST did not improve the regression. This is evident
 646 by visually comparing the observations of Jia and Zhao (2019), which took place in
 647 extremely warm seas ($T_w \sim 28^\circ\text{C}$), to the rest of the data points.

648 4 Discussion

649 4.1 Meteorological Measurements

650 In the previous section, we presented total number concentrations of SSPs
 651 within the Southern Ocean marine boundary layer as measured from two separate
 652 measurement platforms. These were compared to estimations of the total number
 653 concentration of SSPs derived from a source–receptor analysis. To assess the validity
 654 of the meteorological fields used within the source–receptor analysis, we compared
 655 the near-surface winds forecast by AMPS to our observations aboard the R/V *Tan-*
 656 *garooa*. We found that the near-surface winds forecast by AMPS compared favorably
 657 to our observed winds with respect to both magnitude and direction. Previous stud-
 658 ies have found large biases between AMPS forecasts and the true, local winds over
 659 the complex coastal topography of the Antarctic coastline (Bromwich et al., 2005;
 660 Jolly et al., 2016). However, ocean waves have much less surface roughness in com-
 661 parison to the coastal topography of Antarctica, which would suggest that this may
 662 not be as substantial an issue over the ocean.

663 While the precipitation fields forecast by AMPS did not correlate well with
 664 our measurements, the climatological distribution of precipitation events within
 665 AMPS was consistent with our observations. However, within FLEXPART-WRF
 666 a lack of precipitation “trickled up” to the cloud layer: in the current version of
 667 FLEXPART-WRF, clouds are only present within a simulation if they are precip-
 668 itating. As a result, scavenging of SSPs from in-cloud activation was likely poorly
 669 modeled within the AMPS–FLEXPART-WRF framework. As our own observational
 670 record showed, SSPs were strongly scavenged by boundary layer cloud (e.g. fog),
 671 particularly through February 15–17th and March 4–6th, 2018. It is useful, how-
 672 ever, to recall that clouds over the Southern Ocean are not very well represented
 673 within modern atmospheric models (Trenberth & Fasullo, 2010; Schuddeboom et
 674 al., 2019). Current era atmospheric models systematically under-predict the amount
 675 of low-lying cloud and fog relative to the true cloud observed over the Southern
 676 Ocean (Kuma et al., 2019). Hence, even if a state-of-the-art microphysical parame-
 677 terization of in-cloud scavenging had been present in FLEXPART-WRF, it is likely
 678 that the scavenging of sea spray still would have been under-estimated.

679 4.2 Source–Receptor Modelling

680 Once we had established that there was a missing sink of sea spray within our
 681 source–receptor framework, it was necessary to decouple this sink from each of the
 682 parameterizations of surface flux we tested within the regression analysis. This was
 683 accomplished by allowing the simulation length to vary as a free parameter within
 684 the regression analysis. The simulation length can be interpreted as the average
 685 length of time since a boundary layer in-cloud activation event (e.g. fog or low-
 686 cloud). From Table 2 it is evident that our observations were better reproduced for
 687 a fixed simulation length of two days, rather than the five days originally simulated.
 688 This agreed well with the “filling time” of 1.5–2 days used by Ovadnevaite et al.
 689 (2014) to constrain the surface flux of sea spray in the North Atlantic. While setting

690 a voyage-wide simulation time may have been a gross approximation, it was likely
 691 the only approach in light of the present systematic cloud biases over the Southern
 692 Ocean.

693 4.3 Regression Analysis

694 By constraining the missing sink of sea spray within our model framework, we
 695 could finally compare how well the near-surface wind speed and SST predicted our
 696 observational record. We found that the fetch parameterization presented by Xu
 697 et al. (2000) and Snyder and Kennedy (1983) performed the best in our compar-
 698 ison as measured by the Nash-Sutcliffe model efficiency coefficient, NSE, and the
 699 Akaike Information Criterion, AIC. The parameterization, W_F , is so-named since
 700 the parameter c_1 is a function of the fetch. In our analysis we have assumed that
 701 this parameter was constant, since fetch does not significantly influence the degree
 702 of whitecapping in open seas (Hsu, 1986; Piazzola et al., 2002). Later, when we
 703 performed a similar regression analysis with a database of whitecap coverage ob-
 704 servations, we found a slightly smaller value for c_1 . When we compared Eq. (11)
 705 to Eq. (13), we found that c_1 retrieved from the whitecap regression was $6.2 \pm$
 706 0.2 , which was consistent with the value of 6.5 ± 0.2 we retrieved from the SSP re-
 707 gression. The sensitivity of W_F means that Eq. (11) will under-estimate whitecap
 708 coverage globally and subsequently result in under-estimations of sea spray fluxes.
 709 However, we can compare to the value for c_1 retrieved when we only consider South-
 710 ern Ocean whitecap data from Brumer et al. (2017) ($c_1 = 6.4 \pm 0.1$). Combined
 711 with the goodness of fit to the SOCRATES data (Fig. 7a), this provides a secondary
 712 measure of validation for the parameterization over the Southern Ocean. We can
 713 only conclude that for a global study, a value for c_1 of 6.2 may be more appropriate.
 714 For Southern Ocean specific studies a value for c_1 of 6.5 should be used.

715 Finally, we compared results from two other parameterizations for the surface
 716 flux of SSPs to our observations. We found that neither the Jaeglé et al. (2011)
 717 nor the Gong (2003) parameterization could predict the concentration of SSPs we
 718 observed over the Southern Ocean as well as Eq. (11). This is connected to how
 719 the Gong (2003) parameterization (which Jaeglé et al. (2011) re-scaled) scales the
 720 surface flux of SSPs with increasing wind speed. Within this parameterization,
 721 the scaling is estimated via a power-law relationship between the surface coverage
 722 of whitecaps and near-surface wind speed (Monahan & Ó Muircheartaigh, 1980).
 723 However, as we show in Fig. 8b, the parameterization presented by Monahan and
 724 Ó Muircheartaigh (1980) results in consistent over-estimations of the whitecap cov-
 725 erage. These over-estimations propagate through the SSP flux parameterization
 726 of Gong (2003) and lead to the over-estimations in concentrations we observe. In
 727 addition, the power-law predicts that there will always be a flux of sea spray from
 728 the ocean surface, despite it being well-established that whitecaps do not form until
 729 the wind speed over the ocean exceeds $3\text{--}4 \text{ m s}^{-1}$. Even the re-scaled Gong (2003)
 730 parameterization presented in Jaeglé et al. (2011) did not match our observations
 731 well, either.

732 4.4 The Effect of Sea Surface Temperature

733 To understand differences between whitecapping in different regions, previous
 734 research has focused on wave parameters and SST. As Sugihara et al. (2007) and
 735 Goddijn-Murphy et al. (2011) have shown, there is a marked difference between ob-
 736 servations of whitecaps in a pure windsea vs. a swell dominated sea. Indeed, when
 737 we fit W_F to the whitecap data from Sugihara et al. (2007) we retrieved a value
 738 for c_1 of 6.1 ± 0.1 in a pure windsea (indicating higher spatial coverage of white-
 739 capping) compared to 6.7 ± 0.1 when the winds were following swell or counter
 740 swell (indicating lower spatial coverage of whitecapping). This could potentially

741 explain the difference between the value of c_1 we retrieved from our measurements
 742 and the one retrieved from the entire whitecap database. However, conversely, in a
 743 satellite-derived whitecap database, Albert et al. (2016) found that whitecaps were
 744 not dependent on wave parameters, but were actually modestly dependent on SST.
 745 They noted that the lack of dependence on wave parameters may have been a result
 746 of using wind history as a proxy for wave age and spatial averaging. However, we
 747 found that there was no dependence on SST within the database of in situ whitecap
 748 observations.

749 Of course, even if SST does not affect the fractional coverage of whitecaps,
 750 it can still affect the surface flux of particles through changes to viscosity. Re-
 751 sults from laboratory studies are mixed: while two studies have clearly shown that
 752 the surface flux of sea spray should increase in warmer waters (Mårtensson et al.,
 753 2003; Sellegri et al., 2006), others found that that differences in seawater compo-
 754 sition (A. H. Callaghan et al., 2014) and wave characteristics (A. H. Callaghan et
 755 al., 2012) could be much more important. Other laboratory results have even shown
 756 that increases in water temperature led to decreases in sea spray fluxes (Zábori et
 757 al., 2012). To test whether or not changes in SST affected our own observations, we
 758 used SST as a second independent variable within the regression analysis. We found
 759 that the impact to the model-measurement fit was more modest than predicted by
 760 Jaeglé et al. (2011) (see Fig. 7b), and that the parameterization which only used
 761 wind speed (Eq. (11)) performed just as well. As we noted, this may have been a
 762 result of making observations in a very narrow range of SSTs, which would result
 763 in very small changes to the regression metrics we analyzed. However, from Fig. 6b
 764 we can see that the model-measurement residuals don't appear to be significantly
 765 biased from the 1:1 line at warm temperatures.

766 Ultimately, we should be cautious when implementing temperature correction
 767 functions for SSP fluxes. Consider that field observations have already clearly shown
 768 that the presence of swell inhibits the surface fraction of whitecaps for a given wind
 769 speed (Sugihara et al., 2007). Hence, global climatologies of swell could potentially
 770 explain the latitudinal trends in SSP flux expected by (Jaeglé et al., 2011): swell
 771 rarely occurs in the tropics (where fluxes are expected to be higher), whereas swell
 772 frequently is present at high latitudes (where fluxes are expected to be lower) (Jiang
 773 & Chen, 2013). As a result, the resulting bias correction curve Jaeglé et al. (2011)
 774 derived from in situ and satellite observations of aerosol may be partially dependent
 775 on the presence (or absence) of swell. Yet, the curve attributed the latitudinal varia-
 776 tions in flux necessary to fit their observations completely to variations in SST. Our
 777 own observations, which were made exclusively in the presence of swell, showed that
 778 the dependence of SSP fluxes on SST was much weaker than anticipated by Jaeglé
 779 et al. (2011), leading to a very negligible effect on model performance. We conclude
 780 that a more comprehensive global study of sea spray which fully controls for upwind
 781 wave and SST conditions is needed in order to decouple these two effects. In the in-
 782 terim, models should be cautious in implementing functions which could potentially
 783 over-exaggerate radiative feedback loops.

784 4.5 The Direct Radiative Effect

785 As the goal of this study was to understand how SSPs might influence the lo-
 786 cal radiation budget, it would be useful to evaluate whether or not changes to the
 787 parameterization of SSP fluxes result in substantial changes within existing climate-
 788 chemistry models (CCMs). A recent study comparing the winter-time AOD over
 789 the Southern Ocean found that current era parameterizations (e.g. Gong (2003))
 790 of sea spray within a climate-chemistry model (CCM) resulted in over-estimations
 791 of the AOD relative to satellite observations (Revell et al., 2019). However, in the
 792 austral summer, the opposite was observed: namely, a lack of particles formed from

793 the nucleation of sulfate-gasses resulted in under-estimates of AOD. Within this
 794 same study, the parameterization of surface flux, W_{PL} , was implemented within
 795 the CCM to better constrain the contribution of SSPs to the total particle popula-
 796 tion (Revell et al., 2019). While W_{PL} was not the best function determined by this
 797 work, it was similar in form to the Gong (2003) currently implemented within the
 798 CCM being studied, so it was an easy substitution. Since W_{PL} had a Nash-Sutcliffe
 799 coefficient of 0.6 it also produced results that were consistent with Eq. (11). It is
 800 important to note that W_{PL} was used to re-scale the size distribution of the Gong
 801 (2003) parameterization, so any changes would be related to differences in the scal-
 802 ing function and not to differences between size distributions. Results conclusively
 803 showed that the more conservative estimates of the surface flux of SSPs generated
 804 by W_{PL} completely removed the bias in winter-time AOD that was previously ob-
 805 served. Therefore, we are confident that the parameterization for the surface flux of
 806 SSPs presented in Eq. (11) will result in better predictions of the abundance of SSPs
 807 within the Southern Ocean region. More importantly, Revell et al. (2019) show that
 808 it helps disentangle the potential compensating errors in predicting the AOD for
 809 studies interested in the more complicated gas phase and aqueous phase chemistry
 810 which produces sulfate particles from volatile marine precursors like dimethylsulfide.

811 As we have emphasized throughout this study, the MBL over the South-
 812 ern Ocean region is home to the strongest surface winds over open ocean on
 813 Earth (I. Young, 1999). Surface winds also appear to be getting stronger: at Mac-
 814 quarie Island, winds have increased in intensity by 3 cm s^{-1} per year from 1973–
 815 2011, with satellite data showing that winds over the Ross Sea increased by 0.5–1%
 816 through 1991–2008 (Hande et al., 2012; I. R. Young et al., 2011). Within the Ross
 817 Sea region, this increase is related to the deepening of the Amundsen Sea low, an
 818 area of climatologically low pressure in the Southern Ocean which influences regional
 819 winds, sea-ice extent and temperature (Coggins & McDonald, 2015; Raphael et al.,
 820 2016). As we show throughout this study, sea spray has a highly non-linear rela-
 821 tionship with wind speed. Given their large contribution to the CCN population
 822 (10–65%; Quinn et al. (2017)), AOD (Murphy et al., 1998; Revell et al., 2019), and
 823 cloud phase (McCluskey et al., 2018) over the Southern Ocean, these particles can
 824 have a significant buffering effect on the local climate. We would therefore encourage
 825 future studies interested in climate projections for the Southern Ocean to make use
 826 of Eq. (11) when predicting the surface flux of sea spray generated particles.

827 5 Conclusions

828 In this study, we described and optimized an existing parameterization for
 829 the surface flux of sea spray generated particles (SSPs) based on the 10 m wind
 830 speed in Eq. (11). Within our regression framework we found that the dependence
 831 of SSP fluxes on SST was very weak in the temperature range of our observations
 832 ($T_w < 12 \text{ }^\circ\text{C}$) and that it did not help to constrain additional variability in our
 833 data set. An external database of previously published whitecap observations was
 834 exploited to test the parameterization we used in this analysis and found no tem-
 835 perature dependence at all. While others have shown that temperature-dependent
 836 flux parameterizations seem to explain known latitudinal variations in SSP flux, the
 837 correction functions derived from such an analysis could potentially be a proxy for
 838 latitudinal variations in wave characteristics. Given the potential links between SSPs
 839 and the Southern Ocean radiation budget, we should be cautious to add feedback
 840 loops where none may exist.

841 Finally, the parameterization presented in this study is already being used
 842 to model the AOD and concentration of CCN in the region. Research has shown
 843 that the new parameterization vastly improved regional calculations of AOD, com-
 844 pared with previous parameterizations which over-predicted the surface flux of

845 SSPs (Revell et al., 2019). We recommend that studies interested in aerosol–cloud
 846 interactions implement the parameterization as it has been shown to better con-
 847 strain the contribution of SSPs to the CCN population.

848 Acknowledgments

849 This project was funded through the New Zealand Deep South National Science
 850 Challenge Cloud and Aerosols project (2017–19). The Antarctic voyage operations
 851 were supported through a New Zealand Crown Funding Agreement and associated
 852 voyage science was funded through the National Institute of Water and Atmospheric
 853 Research’s Research Programme in Ocean-Climate Interactions (2017/19 SCI).
 854 SOCRATES measurements were supported by award number AGS-1660537 from
 855 the U.S. National Science Foundation. S.P.H. acknowledges support from the Uni-
 856 versity of Canterbury Doctoral Scholarship. D.W.T. acknowledges support from the
 857 University of Canterbury Erskine Programme during a 2018 sabbatical to collab-
 858 orate on this project. L.E.R. was supported by the Deep South National Science
 859 Challenge (grant C01X1412) and acknowledges China Southern for partial support.
 860 K.S. has received funding from the European Research Council (ERC) under the
 861 European Union’s Horizon 2020 research and innovation programme (Sea2Cloud
 862 grant agreement No 771369) for contributing to this work. The authors would like to
 863 acknowledge R/V *Tangaroa* Captain Evan Solly, fellow officers and associated crew
 864 for safe passage throughout the voyage in addition to the fellow sea-going scientific
 865 staff and voyage leader Dr David Bowden. Thanks especially to those talented and
 866 capable crew of the R/V *Tangaroa* who installed both the temporary air inlet and
 867 the container laboratory in which this study was conducted. Additional thanks are
 868 owed to John McGregor and Gordon Brailsford for underway Picarro CO₂ measure-
 869 ments and to Nick Eton for his help troubleshooting technical issues throughout the
 870 voyage.

871 References

- 872 Akaike, H. (1974). A new look at the statistical model identification. *IEEE Transac-*
 873 *tions on Automatic Control*, 19(6), 716–723. doi: 10.1109/TAC.1974.1100705
- 874 Albert, M. F. M. A., Anguelova, M. D., Manders, A. M. M., Schaap, M., & de
 875 Leeuw, G. (2016). Parameterization of oceanic whitecap fraction based on
 876 satellite observations. *Atmospheric Chemistry and Physics*, 16(21), 13725–
 877 13751. doi: 10.5194/acp-16-13725-2016
- 878 Andreas, E. L., Mahrt, L., & Vickers, D. (2015). An improved bulk air–sea surface
 879 flux algorithm, including spray-mediated transfer. *Quarterly Journal of the*
 880 *Royal Meteorological Society*, 141(687), 642–654. doi: 10.1002/qj.2424
- 881 Ayash, T., Gong, S., & Jia, C. Q. (2008). Direct and indirect shortwave radiative ef-
 882 fects of sea salt aerosols. *Journal of Climate*, 21(13), 3207–3220. doi: 10.1175/
 883 2007JCLI2063.1
- 884 Bao, J.-W., Fairall, C. W., Michelson, S. A., & Bianco, L. (2011). Parameteriza-
 885 tions of sea-spray impact on the air–sea momentum and heat fluxes. *Monthly*
 886 *Weather Review*, 139(12), 3781–3797. doi: 10.1175/MWR-D-11-00007.1
- 887 Bell, T. G., Landwehr, S., Miller, S. D., de Bruyn, W. J., Callaghan, A. H., Scanlon,
 888 B., ... Saltzman, E. S. (2017). Estimation of bubble-mediated air–sea gas ex-
 889 change from concurrent DMS and CO₂ transfer velocities at intermediate–high
 890 wind speeds. *Atmospheric Chemistry and Physics*, 17(14), 9019–9033. doi:
 891 10.5194/acp-17-9019-2017
- 892 Bodas-Salcedo, A., Williams, K. D., Ringer, M. A., Beau, I., Cole, J. N., Dufresne,
 893 J.-L., ... Yokohata, T. (2014). Origins of the solar radiation biases over the
 894 Southern Ocean in CFMIP2 models. *Journal of Climate*, 27(1), 41–56.
- 895 Brioude, J., Arnold, D., Stohl, A., Cassiani, M., Morton, D., Seibert, P., ... Wotawa,

- 896 G. (2013). The Lagrangian particle dispersion model FLEXPART-WRF
897 version 3.1. *Geoscientific Model Development*, 6(6), 1889–1904. doi:
898 10.5194/gmd-6-1889-2013
- 899 Brockman, J. (2001). Sampling and transport of aerosols. In P. A. Baron &
900 K. Willeke (Eds.), *Aerosol measurement: Principles, techniques, and applica-*
901 *tions* (2nd ed., pp. 143–197). Hoboken, NJ: John Wiley and Sons, Inc.
- 902 Bromwich, D. H., Monaghan, A. J., Manning, K. W., & Powers, J. G. (2005). Real-
903 time forecasting for the Antarctic: An evaluation of the Antarctic Mesoscale
904 Prediction System (AMPS). *Monthly Weather Review*, 133(3), 579–603. doi:
905 10.1175/MWR-2881.1
- 906 Brumer, S. E., Zappa, C. J., Brooks, I. M., Tamura, H., Brown, S. M., Blomquist,
907 B. W., ... Cifuentes-Lorenzen, A. (2017). Whitecap coverage dependence on
908 wind and wave statistics as observed during so gasex and hiwings. *Journal of*
909 *Physical Oceanography*, 47(9), 2211–2235. doi: 10.1175/JPO-D-17-0005.1
- 910 Burnham, K. P., & Anderson, D. R. (2002). *Model selection and multimodel infer-*
911 *ence* (2nd ed.). Springer-Verlag New York. doi: 10.1007/b97636
- 912 Callaghan, A., de Leeuw, G., Cohen, L., & O’Dowd, C. D. (2008). Relationship
913 of oceanic whitecap coverage to wind speed and wind history. *Geophysical Re-*
914 *search Letters*, 35(23). doi: 10.1029/2008GL036165
- 915 Callaghan, A. H., Deane, G. B., Stokes, M. D., & Ward, B. (2012). Observed vari-
916 ation in the decay time of oceanic whitecap foam. *Journal of Geophysical Re-*
917 *search: Oceans*, 117(C9). doi: 10.1029/2012JC008147
- 918 Callaghan, A. H., Stokes, M. D., & Deane, G. B. (2014). The effect of water tem-
919 perature on air entrainment, bubble plumes, and surface foam in a laboratory
920 breaking-wave analog. *Journal of Geophysical Research: Oceans*, 119(11),
921 7463–7482. doi: 10.1002/2014JC010351
- 922 Callaghan, A. H., & White, M. (2009). Automated processing of sea surface im-
923 ages for the determination of whitecap coverage. *Journal of Atmospheric and*
924 *Oceanic Technology*, 26(2), 383–394. doi: 10.1175/2008JTECHO634.1
- 925 Carslaw, K. S., Lee, L. A., Reddington, C. L., Pringle, K. J., Rap, A., Forster,
926 P. M., ... Pierce, J. R. (2013). Large contribution of natural aerosols to uncer-
927 tainty in indirect forcing. *Nature*, 503, 67–71. doi: 10.1038/nature12674
- 928 Coggins, J. H. J., & McDonald, A. J. (2015). The influence of the Amundsen Sea
929 low on the winds in the Ross Sea and surroundings: Insights from a synoptic
930 climatology. *Journal of Geophysical Research: Atmospheres*, 120(6), 2167–2189.
931 doi: 10.1002/2014JD022830
- 932 Coggins, J. H. J., McDonald, A. J., & Jolly, B. (2014). Synoptic climatology of
933 the Ross Ice Shelf and Ross Sea region of Antarctica: k-means clustering and
934 validation. *International Journal of Climatology*, 34(7), 2330–2348. doi:
935 10.1002/joc.3842
- 936 DeMott, P. J., Hill, T. C. J., McCluskey, C. S., Prather, K. A., Collins, D. B., Sulli-
937 van, R. C., ... Franc, G. D. (2016). Sea spray aerosol as a unique source of ice
938 nucleating particles. *Proceedings of the National Academy of Sciences*, 113(21),
939 5797–5803. doi: 10.1073/pnas.1514034112
- 940 DeMott, P. J., Prenni, A. J., Liu, X., Kreidenweis, S. M., Petters, M. D., Twohy,
941 C. H., ... Rogers, D. C. (2010). Predicting global atmospheric ice nuclei distri-
942 butions and their impacts on climate. *Proceedings of the National Academy of*
943 *Sciences*, 107(25), 11217–11222. doi: 10.1073/pnas.0910818107
- 944 Edson, J. B., Jampana, V., Weller, R. A., Bigorre, S. P., Plueddemann, A. J.,
945 Fairall, C. W., ... Hersbach, H. (2013). On the exchange of momentum over
946 the open ocean. *Journal of Physical Oceanography*, 43(8), 1589–1610. doi:
947 10.1175/JPO-D-12-0173.1
- 948 Fisher, N. I., & Lee, A. J. (1986). Correlation coefficients for random variables on a
949 unit sphere or hypersphere. *Biometrika*, 73(1), 159–164.
- 950 Gerber, H. E. (1985). *Relative-humidity parameterization of the Navy Aerosol Model*

- 951 (NAM) (Tech. Rep.). Washington, DC: Naval Research Lab.
- 952 Goddijn-Murphy, L., Woolf, D. K., & Callaghan, A. H. (2011). Parameterizations
953 and algorithms for oceanic whitecap coverage. *Journal of Physical Oceanogra-*
954 *phy*, *41*(4), 742-756. doi: 10.1175/2010JPO4533.1
- 955 Gong, S. L. (2003). A parameterization of sea-salt aerosol source function for sub-
956 and super-micron particles. *Global Biogeochemical Cycles*, *17*(4). doi: 10.1029/
957 2003GB002079
- 958 Grythe, H., Kristiansen, N. I., Groot Zwaaftink, C. D., Eckhardt, S., Ström, J.,
959 Tunved, P., ... Stohl, A. (2017). A new aerosol wet removal scheme for the
960 Lagrangian particle model FLEXPART v10. *Geoscientific Model Development*,
961 *10*(4), 1447-1466. doi: 10.5194/gmd-10-1447-2017
- 962 Grythe, H., Ström, J., Krejci, R., Quinn, P., & Stohl, A. (2014). A review of
963 sea-spray aerosol source functions using a large global set of sea salt aerosol
964 concentration measurements. *Atmospheric Chemistry and Physics*, *14*(3),
965 1277-1297. doi: 10.5194/acp-14-1277-2014
- 966 Hande, L. B., Siems, S. T., & Manton, M. J. (2012). Observed trends in wind speed
967 over the Southern Ocean. *Geophysical Research Letters*, *39*(11). doi: 10.1029/
968 2012GL051734
- 969 Henzing, J. S., Olivé, D. J. L., & van Velthoven, P. F. J. (2006). A parameteri-
970 zation of size resolved below cloud scavenging of aerosols by rain. *Atmospheric*
971 *Chemistry and Physics*, *6*(11), 3363-3375. doi: 10.5194/acp-6-3363-2006
- 972 Hertel, O., Christensen, J., Runge, E. H., Asman, W. A., Berkowicz, R., Hovmand,
973 M. F., & Øystein Hov. (1995). Development and testing of a new variable scale
974 air pollution model—ACDEP. *Atmospheric Environment*, *29*(11), 1267-1290.
975 doi: [https://doi.org/10.1016/1352-2310\(95\)00067-9](https://doi.org/10.1016/1352-2310(95)00067-9)
- 976 Hicks, B. B., Baldocchi, D. D., Meyers, T. P., Hosker, R. P., & Matt, D. R. (1987).
977 A preliminary multiple resistance routine for deriving dry deposition velocities
978 from measured quantities. *Water, Air, and Soil Pollution*, *36*(3), 311-330. doi:
979 10.1007/BF00229675
- 980 Hsu, S. A. (1986). A mechanism for the increase of wind stress (drag) coefficient
981 with wind speed over water surfaces: A parametric model. *Journal of Phys-*
982 *ical Oceanography*, *16*(1), 144-150. doi: 10.1175/1520-0485(1986)016<0144:
983 AMFTIO>2.0.CO;2
- 984 Hwang, P. A. (2018). High-wind drag coefficient and whitecap coverage derived
985 from microwave radiometer observations in tropical cyclones. *Journal of Physi-*
986 *cal Oceanography*, *48*(10), 2221-2232. doi: 10.1175/JPO-D-18-0107.1
- 987 Jaeglé, L., Quinn, P. K., Bates, T. S., Alexander, B., & Lin, J.-T. (2011). Global
988 distribution of sea salt aerosols: new constraints from in situ and remote sens-
989 ing observations. *Atmospheric Chemistry and Physics*, *11*(7), 3137-3157. doi:
990 10.5194/acp-11-3137-2011
- 991 Jia, N., & Zhao, D. (2019, Apr 01). The influence of wind speed and sea states on
992 whitecap coverage. *Journal of Ocean University of China*, *18*(2), 282-292. doi:
993 10.1007/s11802-019-3808-7
- 994 Jiang, H., & Chen, G. (2013). A global view on the swell and wind sea climate by
995 the Jason-1 mission: A revisit. *Journal of Atmospheric and Oceanic Technol-*
996 *ogy*, *30*(8), 1833-1841. doi: 10.1175/JTECH-D-12-00180.1
- 997 Jolly, B., McDonald, A. J., Coggins, J. H. J., Zawar-Reza, P., Cassano, J., Laz-
998 zara, M., ... Dale, E. (2016). A validation of the Antarctic mesoscale pre-
999 diction system using self-organizing maps and high-density observations
1000 from SNOWWEB. *Monthly Weather Review*, *144*(9), 3181-3200. doi:
1001 10.1175/MWR-D-15-0447.1
- 1002 Kaleschke, L., Richter, A., Burrows, J., Afe, O., Heygster, G., Notholt, J., ... Jacobi,
1003 H.-W. (2004). Frost flowers on sea ice as a source of sea salt and their influ-
1004 ence on tropospheric halogen chemistry. *Geophysical Research Letters*, *31*(16).
1005 doi: 10.1029/2004GL020655

- 1006 Kuma, P., McDonald, A. J., Morgenstern, O., Alexander, S. P., Cassano, J. J., Gar-
 1007 rett, S., ... Williams, J. (2019). Evaluation of Southern Ocean cloud in the
 1008 HadGEM3 general circulation model and MERRA-2 reanalysis using ship-
 1009 based observations. *Atmospheric Chemistry and Physics Discussions*, 2019,
 1010 1–37. doi: 10.5194/acp-2019-201
- 1011 Kyrö, E.-M., Grönholm, T., Vuollekoski, H., Virkkula, A., Kulmala, M., & Laakso,
 1012 L. (2009). Snow scavenging of ultrafine particles: field measurements and
 1013 parameterization. *Boreal Environment Research*, 14, 527–538.
- 1014 Lewis, E., & Schwartz, S. (2004). *Sea salt aerosol production: Mechanisms, methods,
 1015 measurements and models – a critical review*. Washington, DC: American Geo-
 1016 physical Union.
- 1017 McCluskey, C. S., Hill, T. C. J., Humphries, R. S., Rauker, A. M., Moreau, S.,
 1018 Strutton, P. G., ... DeMott, P. J. (2018). Observations of ice nucleating
 1019 particles over Southern Ocean waters. *Geophysical Research Letters*, 45(21),
 1020 11,989–11,997. doi: 10.1029/2018GL079981
- 1021 McCoy, D. T., Burrows, S. M., Wood, R., Grosvenor, D. P., Elliott, S. M., Ma,
 1022 P.-L., ... Hartmann, D. L. (2015). Natural aerosols explain seasonal and spa-
 1023 tial patterns of Southern Ocean cloud albedo. *Science Advances*, 1(6). doi:
 1024 10.1126/sciadv.1500157
- 1025 Modini, R. L., Frossard, A. A., Ahlm, L., Russell, L. M., Corrigan, C. E., Roberts,
 1026 G. C., ... Leaitch, W. R. (2015). Primary marine aerosol-cloud interactions off
 1027 the coast of California. *Journal of Geophysical Research: Atmospheres*, 120(9),
 1028 4282–4303. doi: 10.1002/2014JD022963
- 1029 Monahan, E. C. (1971). Oceanic whitecaps. *Journal of Physical Oceanography*, 1(2),
 1030 139–144. doi: 10.1175/1520-0485(1971)001<0139:OW>2.0.CO;2
- 1031 Monahan, E. C., Spiel, D. E., & Davidson, K. L. (1986). A model of marine aerosol
 1032 generation via whitecaps and wave disruption. In E. C. Monahan & G. M. Nio-
 1033 caill (Eds.), *Oceanic whitecaps: And their role in air-sea exchange processes*
 1034 (pp. 167–174). Dordrecht: Springer. doi: 10.1007/978-94-009-4668-2_16
- 1035 Monahan, E. C., & Ó Muircheartaigh, I. (1980). Optimal power-law description
 1036 of oceanic whitecap coverage dependence on wind speed. *Journal of Physical
 1037 Oceanography*, 10(12), 2094–2099. doi: 10.1175/1520-0485(1980)010<2094:
 1038 OPLDOO>2.0.CO;2
- 1039 Murphy, D., Anderson, J., Quinn, P., McInnes, L., Brechtel, F., Kreidenweis, S.,
 1040 ... Buseck, P. (1998). Influence of sea-salt on aerosol radiative properties
 1041 in the Southern Ocean marine boundary layer. *Nature*, 392, 62–65. doi:
 1042 10.1038/32138
- 1043 Mårtensson, E. M., Nilsson, E. D., de Leeuw, G., Cohen, L. H., & Hansson, H.-C.
 1044 (2003). Laboratory simulations and parameterization of the primary marine
 1045 aerosol production. *Journal of Geophysical Research: Atmospheres*, 108(D9).
 1046 doi: 10.1029/2002JD002263
- 1047 Nash, J., & Sutcliffe, J. (1970). River flow forecasting through conceptual models
 1048 part i — a discussion of principles. *Journal of Hydrology*, 10(3), 282 - 290. doi:
 1049 10.1016/0022-1694(70)90255-6
- 1050 Norris, S. J., Brooks, I. M., Moat, B. I., Yelland, M. J., de Leeuw, G., Pascal,
 1051 R. W., & Brooks, B. (2013). Near-surface measurements of sea spray
 1052 aerosol production over whitecaps in the open ocean. *Ocean Science*, 9(1),
 1053 133–145. Retrieved from <https://www.ocean-sci.net/9/133/2013/> doi:
 1054 10.5194/os-9-133-2013
- 1055 Ortiz-Suslow, D. G., Haus, B. K., Mehta, S., & Laxague, N. J. M. (2016). Sea spray
 1056 generation in very high winds. *Journal of the Atmospheric Sciences*, 73(10),
 1057 3975–3995. doi: 10.1175/JAS-D-15-0249.1
- 1058 Ovadnevaite, J., Manders, A., de Leeuw, G., Ceburnis, D., Monahan, C., Partanen,
 1059 A.-I., ... O’Dowd, C. D. (2014). A sea spray aerosol flux parameterization en-
 1060 capsulating wave state. *Atmospheric Chemistry and Physics*, 14(4), 1837–1852.

- doi: 10.5194/acp-14-1837-2014
- 1061
1062 Petters, M. D., & Kreidenweis, S. M. (2007). A single parameter representation
1063 of hygroscopic growth and cloud condensation nucleus activity. *Atmospheric*
1064 *Chemistry and Physics*, 7(8), 1961–1971. doi: 10.5194/acp-7-1961-2007
- 1065 Piazzola, J., Forget, P., & Despiau, S. (2002). A sea spray generation function for
1066 fetch-limited conditions. *Annales Geophysicae*, 20(1), 121–131. doi: 10.5194/
1067 angeo-20-121-2002
- 1068 Polar Meteorology Group, Byrd Polar and Climate Research Center. (2018, 7 17).
1069 *Antarctic mesoscale prediction system (AMPS) domain 1 forecasts*. data re-
1070 trieved from Climate Data Gateway at NCAR. Retrieved 17/7/2018, from
1071 <https://www.earthsystemgrid.org/project/amps.html>
- 1072 Popinet, S., Smith, M., & Stevens, C. (2004). Experimental and numerical
1073 study of the turbulence characteristics of airflow around a research vessel.
1074 *Journal of Atmospheric and Oceanic Technology*, 21(10), 1575–1589. doi:
1075 10.1175/1520-0426(2004)021<1575:EANSOT>2.0.CO;2
- 1076 Powell, M. D., Vickery, P. J., & Reinhold, T. A. (2003). Reduced drag coefficient
1077 for high wind speeds in tropical cyclones. *Nature*, 422(6929), 279–283. doi: 10
1078 .1038/nature01481
- 1079 Prather, K. A., Bertram, T. H., Grassian, V. H., Deane, G. B., Stokes, M. D., De-
1080 Mott, P. J., ... Zhao, D. (2013). Bringing the ocean into the laboratory to
1081 probe the chemical complexity of sea spray aerosol. *Proceedings of the National*
1082 *Academy of Sciences*, 110(19), 7550–7555. doi: 10.1073/pnas.1300262110
- 1083 Quinn, P. K., Coffman, D. J., Johnson, J. E., Upchurch, L. M., & Bates, T. S.
1084 (2017). Small fraction of marine cloud condensation nuclei made up of sea
1085 spray aerosol. *Nature Geoscience*, 10, 674–679. doi: 10.1038/ngeo3003
- 1086 Raphael, M. N., Marshall, G. J., Turner, J., Fogt, R. L., Schneider, D., Dixon,
1087 D. A., ... Hobbs, W. R. (2016). The Amundsen Sea low: Variability, change,
1088 and impact on Antarctic climate. *Bulletin of the American Meteorological*
1089 *Society*, 97(1), 111-121. doi: 10.1175/BAMS-D-14-00018.1
- 1090 Revell, L. E., Kremser, S., Hartery, S., Harvey, M., Mulcahy, J. P., Williams, J.,
1091 ... Schuddeboom, A. (2019). The sensitivity of Southern Ocean aerosols
1092 and cloud microphysics to sea spray and sulfate aerosol production in the
1093 HadGEM3-GA7.1 chemistry-climate model. *Atmospheric Chemistry and*
1094 *Physics Discussions*, 2019, 1–36. Retrieved from <https://www.atmos-chem>
1095 [-physics-discuss.net/acp-2019-629/](https://www.atmos-chem-physics-discuss.net/acp-2019-629/) doi: 10.5194/acp-2019-629
- 1096 Richter, D. H., & Sullivan, P. P. (2013). Sea surface drag and the role of spray. *Geo-*
1097 *physical Research Letters*, 40(3), 656–660. doi: 10.1002/grl.50163
- 1098 Schuddeboom, A., Varma, V., McDonald, A. J., Morgenstern, O., Harvey, M., Par-
1099 sons, S., ... Furtado, K. (2019). Cluster-based evaluation of model compen-
1100 sating errors: A case study of cloud radiative effect in the Southern Ocean.
1101 *Geophysical Research Letters*, 46(6), 3446-3453. doi: 10.1029/2018GL081686
- 1102 Schwendeman, M., & Thomson, J. (2015). Observations of whitecap cover-
1103 age and the relation to wind stress, wave slope, and turbulent dissipa-
1104 tion. *Journal of Geophysical Research: Oceans*, 120(12), 8346-8363. doi:
1105 10.1002/2015JC011196
- 1106 Sellegri, K., O’Dowd, C. D., Yoon, Y. J., Jennings, S. G., & de Leeuw, G. (2006).
1107 Surfactants and submicron sea spray generation. *Journal of Geophysical Re-*
1108 *search: Atmospheres*, 111(D22). doi: 10.1029/2005JD006658
- 1109 Shindell, D. T., Lamarque, J.-F., Schulz, M., Flanner, M., Jiao, C., Chin, M., ... Lo,
1110 F. (2013). Radiative forcing in the ACCMIP historical and future climate
1111 simulations. *Atmospheric Chemistry and Physics*, 13(6), 2939–2974. doi:
1112 10.5194/acp-13-2939-2013
- 1113 Slinn, W. (1977). Some approximations for the wet and dry removal of particles and
1114 gases from the atmosphere. *Water, Air, and Soil Pollution*, 7(4), 513–543. doi:
1115 10.1007/BF00285550

- 1116 Smith, M. J., Ho, D. T., Law, C. S., McGregor, J., Popinet, S., & Schlosser, P.
 1117 (2011). Uncertainties in gas exchange parameterization during the SAGE dual-
 1118 tracer experiment. *Deep Sea Research Part II: Topical Studies in Oceanogra-*
 1119 *phy*, 58(6), 869 - 881. doi: 10.1016/j.dsr2.2010.10.025
- 1120 Snyder, R. L., & Kennedy, R. M. (1983). On the formation of whitecaps
 1121 by a threshold mechanism. part i: basic formalism. *Journal of Physical*
 1122 *Oceanography*, 13(8), 1482-1492. doi: 10.1175/1520-0485(1983)013<1482:
 1123 OTFOWB>2.0.CO;2
- 1124 Stramska, M., & Petelski, T. (2003). Observations of oceanic whitecaps in the
 1125 north polar waters of the atlantic. *Journal of Geophysical Research: Oceans*,
 1126 108(C3). doi: 10.1029/2002JC001321
- 1127 Sugihara, Y., Tsumori, H., Ohga, T., Yoshioka, H., & Serizawa, S. (2007). Vari-
 1128 ation of whitecap coverage with wave-field conditions. *Journal of Marine Sys-*
 1129 *tems*, 66(1), 47 - 60. (5th International Symposium on Gas Transfer at Water
 1130 Surfaces) doi: <https://doi.org/10.1016/j.jmarsys.2006.01.014>
- 1131 Trenberth, K. E., & Fasullo, J. T. (2010). Simulation of present-day and twenty-
 1132 first-century energy budgets of the Southern Oceans. *Journal of Climate*,
 1133 23(2), 440-454.
- 1134 Twomey, S. (1977). The influence of pollution on the shortwave albedo of
 1135 clouds. *Journal of the Atmospheric Sciences*, 34(7), 1149-1152. doi:
 1136 10.1175/1520-0469(1977)034<1149:TIOPO>2.0.CO;2
- 1137 Witek, M. L., Diner, D. J., & Garay, M. J. (2016). Satellite assessment of sea spray
 1138 aerosol productivity: Southern Ocean case study. *Journal of Geophysical Re-*
 1139 *search: Atmospheres*, 121(2), 872-894. doi: 10.1002/2015JD023726
- 1140 Xu, D., Liu, X., & Yu, D. (2000). Probability of wave breaking and whitecap cover-
 1141 age in a fetch-limited sea. *Journal of Geophysical Research: Oceans*, 105(C6),
 1142 14253-14259. doi: 10.1029/2000JC900040
- 1143 Yang, X., Pyle, J. A., & Cox, R. A. (2008). Sea salt aerosol production and bromine
 1144 release: Role of snow on sea ice. *Geophysical Research Letters*, 35(16). doi: 10
 1145 .1029/2008GL034536
- 1146 Young, I. (1999). Seasonal variability of the global ocean wind and wave climate.
 1147 *International Journal of Climatology*, 19(9), 931-950. doi: 10.1002/(SICI)1097
 1148 -0088(199907)19:9<931::AID-JOC412>3.0.CO;2-O
- 1149 Young, I. R., Zieger, S., & Babanin, A. V. (2011). Global trends in wind speed and
 1150 wave height. *Science*, 332(6028), 451-455. doi: 10.1126/science.1197219
- 1151 Zábori, J., Krejci, R., Ekman, A. M. L., Mårtensson, E. M., Ström, J., de Leeuw,
 1152 G., & Nilsson, E. D. (2012). Wintertime Arctic Ocean sea water proper-
 1153 ties and primary marine aerosol concentrations. *Atmospheric Chemistry and*
 1154 *Physics*, 12(21), 10405-10421. doi: 10.5194/acp-12-10405-2012